NACA

RESEARCH MEMORANDUM

INVESTIGATION OF THE JET EFFECTS ON A FLAT SURFACE DOWNSTREAM OF THE EXIT OF A SIMULATED TURBOJET NACELLE AT A FREE-STREAM MACH NUMBER OF 2.02

By Walter E. Bressette

Langley Aeronautical Laboratory
Langley Field, Va.

NATIONAL ADVISORY COMMITTEE
FOR AERONAUTICS

WASHINGTON

June 23, 1954
Declassified May 8, 1957

NATIONAL ADVISORY COMMITTEE FOR AERONAUTICS

RESEARCH MEMORANDUM

INVESTIGATION OF THE JET EFFECTS ON A FLAT SURFACE DOWNSTREAM OF THE EXIT OF A SIMULATED TURBOJET NACELLE AT A FREE-STREAM MACH NUMBER OF 2.02

By Walter E. Bressette

SUMMARY

An investigation at a free-stream Mach number of 2.02 was made to determine the effects of a propulsive jet on a wing surface located in the vicinity of a choked convergent nozzle. Static-pressure surveys were made on a flat surface that was located in the vicinity of the propulsive jet. The nozzle was operated over a range of exit pressure ratios at different fixed vertical distances from the flat surface.

Within the scope of this investigation, it was found that shock waves, formed in the external flow because of the presence of the propulsive jet, impinged on the flat surface and greatly altered the pressure distribution. An integration of this pressure distribution, with the location of the propulsive jet exit varied from 1.450 propulsive-jet exit diameters to 3.392 propulsive-jet exit diameters below the wing, resulted in an incremental lift for all jet locations that was equal to the gross thrust at an exit pressure ratio of 2.86.

This incremental lift increased with increase in exit pressure ratio, but not so rapidly as the thrust increased, and was approximately constant at any given exit pressure ratio.

INTRODUCTION

It has been shown in reference 1 that a propulsive jet issuing from the rear of a body at supersonic speeds produced strong disturbances which were responsible for the formation of shock waves in the external flow downstream of the jet exit. It could thus be expected that the induced forces produced by the impingement of these shock waves on downstream surfaces might be of considerable importance. In the past, aircraft designers avoided this problem by placing all surfaces outside of a predetermined blast cone from the propulsive exit. However, at

supersonic speeds, in order to eliminate these induced forces, it would be necessary to keep all surfaces not only away from the propulsive jet itself, but also away from all shock waves in the external flow because of the presence of the propulsive jet. In many cases, with the increased use of delta-wing configurations and longer afterbodies, it is becoming more difficult to do this. This report is concerned with the jet effects produced on an adjacent plane surface by the interaction of the external flow and the propulsive-jet wake, downstream of the jet exit.

The investigation was conducted in the preflight jet of the Langley Pilotless Aircraft Research Station at Wallops Island, Va., by using a small-scale nacelle simulating a turbojet engine that was vertically adjustable beneath a flat surface simulating a wing. Simulation of the density and velocity of a hot exhaust jet was accomplished by using helium. Helium, because of its high gas constant, when used at atmospheric temperature will produce a jet density and velocity comparable to a hot exhaust jet.

The data presented were obtained over a range of jet pressure ratios from 2 to 7 at a free-stream Mach number of 2.02 and at angles of attack and yaw of 0°. The Reynolds number per inch for these tests was 1.22×10^{6}.

SYMBOLS

a chordwise distance from nacelle exit, in. (downstream is positive)

b spanwise distance from nacelle center line, in. (located on wing surface)

C_{L_i} incremental lift coefficient, $\dfrac{(\text{Lift})_n - (\text{Lift})_f}{q_o S_j}$

x_{cp} incremental-lift center-of-pressure location from nacelle exit, in. (downstream is positive)

C_T gross thrust coefficient, $\dfrac{T}{q_o S_j}$

D diameter, in.

H total pressure, lb/sq in.

H_j/p_o nacelle-exit pressure ratio

M Mach number

p static pressure, lb/sq in.

P pressure coefficient, $\frac{p_w - p_o}{q_o}$

q dynamic pressure, $\frac{\gamma p M^2}{2}$, lb/sq in.

r radius of nacelle afterbody at x distance, in.

S area, sq in.

T gross thrust, $\gamma p_j M_j^2 S_j + p_j S_j - p_o S_j$, lb

x horizontal distance along nacelle afterbody, in.

α secondary jet-on wave angle, deg

γ specific heat ratio, 1.40 for air and 1.67 for helium

θ primary jet-on wave angle, deg

Subscripts:

f propulsive jet off

j nacelle exit

n propulsive jet on

o free stream

w wing

APPARATUS

The tests were made in the preflight jet of the Langley Pilotless Aircraft Station at Wallops Island, Va. (ref. 2). A Mach number 2.02, 12-inch-square preflight jet nozzle was used for all tests. A photograph of the nacelle mounted beneath the flat-surface wing in the 12- by 12-inch preflight-jet nozzle is shown as figure 1.

Nacelle.- In figure 2 is shown a sketch of the nacelle with its principal dimensions. Also shown in figure 2 is a 10° canted down nozzle that was included in the tests. The body of the nacelle had a maximum diameter of 1.125 inches with an overall length of 10.50 inches. It was mounted on a hollow strut which served as a housing for the helium conduits and a pressure lead as well as a support for the nacelle. The strut was swept back 45° from the nacelle center line and it had a cross section as shown in figure 2. The dimensions of the nacelle as a whole were scaled down from a full-size typical turbojet nacelle. The coordinates for the afterbody of the nacelle are given in table I.

Wing.- The wing used in the tests consisted of a 1/4-inch-thick stainless-steel plate that completely spanned the exit of the preflight jet nozzle. The wing was welded to supports that were bolted to the exit of the preflight jet nozzle with the leading edge 1/4 inch from the nozzle exit and approximately three-quarters of the total vertical distance up from the bottom. The wing was of rectangular plan form with a 9.25-inch chord and a 14° bevel on the upper surface of the leading edge.

A sketch showing the location of the nacelle with respect to the wing and preflight-jet-nozzle exit for all the positions tested is presented in figure 3. Also shown in figure 3 is the location of the exit center line for the 10° canted down nozzle at position B.

INSTRUMENTATION

The internal static pressure of the nacelle was measured through a 0.03-inch-diameter orifice shown in figure 2.

The static pressure on the wing was measured through 18 static-pressure orifices 0.06 inch in diameter. The position of each of these orifices located from the nacelle exit is shown in figure 4.

Also measured were the free-stream total pressure in the chamber just in front of the preflight-jet-nozzle exit and the stream static pressure on the wall 1/2 inch upstream from this exit. All pressures were recorded by electrical pressure recorders of the strain-gage type. A 10-cps timer correlated all time histories on paper records. Shadowgraphs, which were photographed at an exposure of approximately 0.003 second, were obtained by using a carbon-arc light source and an opaque-glass screen.

ACCURACY

By accounting for the instrument error of 1 percent of full-scale range, the probable error is believed to be within the following limits:

M_o	± 0.02
P_f and P_n	± 0.02
H_j/p_o	± 0.20

The angles θ and α are believed to be accurate to $\pm 1^\circ$.

TEST AND METHODS

The tests were made at a free-stream Mach number of 2.02 with a Reynolds number per inch of 1.22×10^6 while varying the nacelle-exit pressure ratio from 2 to 7.

With the arrangement shown in figure 3, the complete test field was within the Mach wedge of the nozzle and the upper quarter of nozzle flow with its boundary layer was separated out. For all tests, the nacelle-exit center line was located vertically below the center line of the wing at 6.63 inches from the trailing edge. The only variation between individual tests was the vertical distance between wing and nacelle center line as shown in figure 3. At all times, the nacelle was at angles of attack and yaw of 0° with respect to both the wing surface and the center line of the preflight jet.

Helium, from a pressurized source, was used to simulate the propulsive jet from the sonic exit of a turbojet with afterburner operation. Helium was chosen for simulation because its density and sonic velocity most nearly duplicate those of the turbojet exhaust without the complication of heating or mixing of gases. Helium, with its high gas constant, when used at atmospheric temperature will duplicate a hot-exhaust-jet density. However, because of its high specific-heat ratio, the sonic velocity is approximately 10 percent in error. The variation of nacelle-exit pressure ratio was accomplished by allowing the pressure of the helium source to be exhausted.

The total pressure at the nacelle exit was calculated from the measured static pressure by assuming both a sonic exit and lq pressure loss between the static-pressure-orifice location and the exit.

The gross thrust of the propulsive jet was calculated by using the one-dimensional flow theory applied to the momentum-theory equation as follows:

$$T = \gamma p_j M_j^2 S_j + p_j S_j - p_o S_j$$

For a sonic exit,

$$T = p_j S_j(\gamma + 1) - p_o S_j$$

The incremental lift due to the presence of the propulsive jet was determined from an integration of the measured pressures on the lower wing surface. The assumptions and details of this calculation are discussed in the appendix.

RESULTS AND DISCUSSION

Pressure Coefficients

Jet off.- The measured jet-off pressure coefficients P_f on the wing surface are plotted in figure 5 as a function of distance from the nacelle exit a/D_j for three spanwise positions. The chordwise pressure distributions on the wing for positions B, C, and D along the nacelle center line (fig. 5(a)) are characterized first by the expansion to a low pressure region near the vicinity of the exit of the nacelle and, second, by a pressure rise through the shock wave originating from the nacelle wake (fig. 6). As the nacelle is lowered from position B, the low pressure regions, although moved farther to the rear on the wing, are of the same magnitude. In turn, the pressure rise through the shock waves also takes place farther to the rear on the wing and the profiles are generally of the same shape, although the maximum pressure rise is reduced. The reduction in the maximum pressure as the spanwise distance is increased from the nacelle center line (compare figs. 5(a) and 5(b)) also indicates that the pressure rise across the shock wave becomes less intense as its distance from the point of origin to the point of impingement with the wing surface is increased.

With the nacelle in positions A and B (exit canted 10° down), the chordwise pressure profiles on the wing along the nacelle center line (fig. 5(a)) are different from those presented for the other positions. The greatest differences occur in the magnitude of the low pressure field and the general shape and position of the maximum pressure rise

on the wing. The low pressure field for position A is nearly twice that of the other straight-exit positions; this result indicates that the flow between the body of the nacelle and the wing on the nacelle center line for position A is blocked off and forces the flow over the nacelle to detour around before reaching the exit. The effects from this blockage of the flow on the nacelle center line could be expected to be relieved at the spanwise positions indicated by the plots of position A in figures 5(b) and 5(c).

Position B (exit canted 10° down) has the lowest pressure field of all. Although the center line at the point of the exit in position B (exit canted) coincides with the center line of position B (exit straight), actually the body of the nacelle was between positions A and B and this position plus the difference in external shape could be expected to cause a lower pressure at the exit of the model.

Jet on.- Presented in figure 7 (parts (a) to (j)) are the experimental jet-on pressure coefficients P_n for individual orifice locations plotted as a function of nacelle-exit pressure ratio H_j/p_o. The interaction on the wing of the jet-on shock waves shown in the shadowgraph pictures (fig. 8) is responsible for the high positive pressure coefficients, and the movement of these shock waves with an increase in H_j/p_o causes the sudden increase or decrease of P_n for individual orifices. A typical example is the plot of P_n for the orifice located at $a/D_j = 2.88$ in figure 7(e). From $H_j/p_o = 6$ to $H_j/p_o = 3.5$ the shock wave is downstream of the orifice and at $H_j/p_o = 3.5$ it begins to pass over the orifice and causes a rapid pressure rise to a positive pressure until it has finally passed over at $H_j/p_o = 4.5$. Another noticeable effect at this orifice location is the further increase in P_n with an increase in H_j/p_o even though the shock wave has passed over the orifice and is continuing to get farther upstream of it. This increase in P_n and the increased angle of the shock waves (shown subsequently) indicates the increase in the strength of the primary shock wave with an increase in H_j/p_o.

In figure 9, the chordwise variation of P_n is plotted as a function of distance from the nacelle exit a/D_j for test positions A, B, C, and D at H_j/p_o of 6. As can be seen by comparing figure 9 with figure 5, the chordwise wing pressure profiles are the same both with jet on and jet off prior to the initial jet-on pressure rise. After this point, they are distinctly different. With jet on, there are two separate positive pressure rises on the wing at each position. These positive pressure peaks are caused by the interaction on the wing of both a primary and a secondary shock wave visible in the jet-on shadowgraph pictures in figure 8.

Figure 9 also shows, as did figure 5, a reduction in the maximum positive pressure and a rearward movement of the complete pressure profile as the model is lowered in position as well as a reduction at each position as the spanwise distance is increased. This reduction at each position as the spanwise distance is increased as well as the impingement on the wing of both the primary and secondary shock waves is shown in a sketch of a typical jet-on pressure field on the wing presented in figure 10.

Presented in figure 11 is the chordwise variation of the jet-on pressure coefficient on the wing along the nacelle center line for positions B with a straight exit, and B with the exit canted 10° down at $H_j/p_o = 6$. Positions B with a straight exit and B with a canted exit have similar P_n profiles with position B with the exit canted having a sizably lower initial pressure and a slight increase in maximum positive pressure.

Shock Waves

From the shadowgraph pictures in conjunction with the measured wing pressure data over the nacelle center line, it was possible to locate the point of impingement of the shock waves on the flat-surface wing. The angular variation between the wing surface and a straight line drawn along the shock wave was then measured; it represents the angular variation between the nacelle center line and the shock wave. In the jet-off case, only one shock wave, with a mean angle of 29°, impinged on the wing as shown by the pressure rise in figure 5 and the shadowgraph pictures in figure 6. In the jet-on case, two shock waves impinged on the wing as shown by the pressure rises in figure 9 and the shadowgraph pictures in figure 8. The variation of these jet-on wave angles with H_j/p_o is presented in figure 12. The primary shock-wave angle θ, caused by the initial expansion of the propulsive jet from the nacelle exit, had a fixed origin at the exit of the nacelle, and varied from approximately 30° at $H_j/p_o = 2$ to approximately 35° at $H_j/p_o = 7$. This variation in wave angle with H_j/p_o could be expected because increasing the pressure ratio results in an increase in the expansion of the jet issuing from the nacelle exit (ref. 1). The secondary power-on shock wave, although moving farther downstream with an increase in H_j/p_o (fig. 8), appeared to have a constant wave angle α of 31°.

Incremental Lift

Shown in figure 13 is the variation of incremental lift coefficient C_{L_i}, based on S_j, with H_j/p_o for all test positions. The values of C_{L_i} were calculated from the incremental pressure data ($P_n - P_f$) by the

method presented in the appendix; C_{L_i} represents the change in lift due to the presence of the propulsive jet. At positions B, C, and D, the variation of C_{L_i} with H_j/p_o was approximately the same. Values of C_{L_i} varied from approximately 0.80 at $H_j/p_o = 2$ to approximately 1.84 at $H_j/p_o = 7$. When jet-on and jet-off wing pressure data were combined to form the incremental pressure data (fig. 14), positive incremental pressure resulted immediately behind the jet-on primary shock. This positive incremental pressure gradually decreased until it became negative in the vicinity of the jet-off shock and it remained negative in the jet-off shock field to the end of the wing. With the lowering of the nacelle from position B, the intensity and area of the positive incremental pressure field were reduced, but the area of the negative field was also reduced. When both positive and negative pressure fields were combined the resulting incremental lift showed no variation between positions B, C, and D for a given H_j/p_o. Positions A and B (exit canted 10° down) did not produce lift equal to the other positions for a given value of H_j/p_o. The reasons are explained at the end of the appendix, and because it is believed that the method of calculating the incremental lift does not fully apply in these positions, the results therefore serve only as an indication and the curves for positions A and B (exit canted 10° down) are presented as dashed in all the figures.

Incremental-lift center of pressure.- Presented in figure 15 is the variation of the incremental-lift center of pressure (x_{cp}/D_j) with H_j/p_o. The center of pressure at positions B, C, and D is downstream of the nacelle exit at $H_j/p_o = 2$ and shows a gradual movement farther downstream with an increase in H_j/p_o. The gradual movement of the center of pressure farther downstream is the result of the fact that the jet-on secondary shock moves downstream with H_j/p_o and reduces the negative incremental pressure in the jet-off shock field (fig. 14). In positions A and B (exit canted 10° down), the negative incremental pressure fields are proportionately greater than at the other positions but the positive incremental pressure field is not. When both the positive incremental pressure and the negative incremental pressure with their respective center-of-pressure locations are combined in positions A and B (exit canted 10° down), then the resultant center of pressure moves well upstream of the nacelle exit with a reduction in H_j/p_o.

Thrust.- The variation in calculated gross thrust coefficient C_T, based on S_j, is presented in figure 16 plotted against H_j/p_o. Shown in figure 17 is the variation in the incremental lift-to-thrust ratio with H_j/p_o. It can be seen in positions B, C, and D that incremental lift equal to the gross thrust was encountered at $H_j/p_o \approx 2.86$.

The incremental lift-to-thrust ratio decreased rapidly from approximately 1.45 at $H_j/p_o = 2$ to 0.65 at $H_j/p_o = 6$ and then appeared to level out. Positions A and B (exit canted 10° down) again show the effects of severe nacelle-wing interference by having an incremental lift-to-thrust ratio that is gradually increasing with H_j/p_o.

CONCLUDING REMARKS

Within the limits of the present tests conducted in a Mach number 2.02 free jet of a small-scale simulated turbojet nacelle with a choked convergent nozzle located in the near vicinity of a flat-surface wing the results may be summarized as follows:

1. When the position of the center line of the straight-exit nacelle was lowered relative to the wing from 1.450 nacelle exit diameters to 3.392 nacelle exit diameters the following effects were obtained:

   a. The change in pressures on the wing, from the presence of the propulsive jet, when integrated over the affected wing area produced an incremental lift that was equal to the gross thrust at a nacelle-exit pressure ratio of approximately 2.86.

   b. For any given nacelle-exit pressure ratio the incremental lifting effect on the wing was approximately independent of vertical position.

   c. The incremental lift on the wing was increased when the nacelle-exit pressure ratio was increased, but not so rapidly as the thrust increased.

   d. The incremental-lift center of pressure is progressively farther downstream of the nacelle exit as the nacelle was lowered in position, and it moved gradually farther downstream at each position with an increase in the nacelle-exit pressure ratio.

2. The tests of a straight exit at 0.817 nacelle-exit diameters and a canted exit at 1.450 nacelle-exit diameters below the wing indicated lower incremental lift than at the other positions referred to in conclusion 1. Also, at these positions a rapid movement of the incremental-lift center of pressure from well forward of the nacelle exit to slightly behind it occurred with an increase in the nacelle-exit pressure ratio.

Langley Aeronautical Laboratory,
National Advisory Committee for Aeronautics,
Langley Field, Va., April 30, 1954.

APPENDIX

DETERMINATION OF INCREMENTAL LIFT

The following method of determining the incremental lift on a flat-surface wing, resulting from the intersection on the wing of shock waves, due to the presence of the propulsive jet, is based on the assumption that the incremental pressure on the wing decreases in proportion to the distance from the shock-wave source. In figure 14, the validity of the assumption was checked by plotting the limited spanwise experimental incremental pressures on constructed profiles, reduced proportionally with distance, from the center-line profile. The agreement between the constructed profiles and the actual data is shown to be good. Figure 14 is a three-dimensional plot that illustrates the results of the method used in obtaining the incremental lift on the wing. The boundaries of the intersection on the wing of the jet-off and jet-on shock fields were determined by measuring the shock-wave angle from the shadowgraph pictures at $a/D_j = 0$ and then projecting a cone with this half angle on the wing surface. The experimental incremental pressure coefficients were then plotted at $b/D_j = 0$ and the profile between the points was faired in. The strip incremental lift at $b/D_j = 0$ was then determined by integrating the area under the center-line incremental pressure profile. From the strip incremental lift at $b/D_j = 0$, the strip incremental lift at any spanwise station can be obtained by reducing the strip incremental lift at $b/D_j = 0$ in proportion to the increase in distance to the spanwise wing position from the shock-wave source. By integrating the lift per chordwise strip from $b/D_j = 0$ to $b/D_j = \text{Maximum}$ and multiplying by 2, the incremental lift on the wing can be obtained. A pressure orifice on the wing located at $3.04D_j$ spanwise and $2.88D_j$ chordwise from the nacelle exit, opposite in spanwise position from the main pressure survey (fig. 4), showed good agreement in incremental pressure with its identically located orifice in the main pressure survey.

For positions B, C, and D, the agreement between the experimental incremental pressures and the constructed profiles is consistently good throughout, but for position A the agreement is not so good. In some cases, the limited incremental pressures at the spanwise station $b/D_j = 1.35$ were approximately 30 to 40 percent higher than the constructed profiles. The flow being blocked between the wing and nacelle at $b/D_j = 0$ for position A could be responsible for this inaccuracy in the method by causing the flow to detour away from the $b/D_j = 0$ position. The agreement between spanwise experimental incremental pressures and the constructed profiles at position B with a canted exit is nearly as

good as it was at position B with a straight exit, but since the method of obtaining the lift is based on a symmetrical nacelle exit about the nacelle center line, this agreement would not be expected to continue over all spanwise positions for position B with a canted exit as it could be for position B with a straight exit.

REFERENCES

1. Rousso, Morris D., and Baughman, L. Eugene: Investigation at Mach Number 1.91 of Spreading Characteristics of Jet Expanding From Choked Nozzles. NACA RM E51L19, 1952.

2. Faget, Maxime A., Watson, Raymond S., and Bartlett, Walter A., Jr.: Free-Jet Tests of a 6.5-Inch-Diameter Ram-Jet Engine at Mach Numbers of 1.81 and 2.00. NACA RM L50L06, 1951.

TABLE I

AFTERBODY COORDINATES

x, in.	r, in.
0	0.56
.50	.54
1.00	.53
1.50	.51
2.00	.47
2.50	.43
3.00	.39
3.27	.37

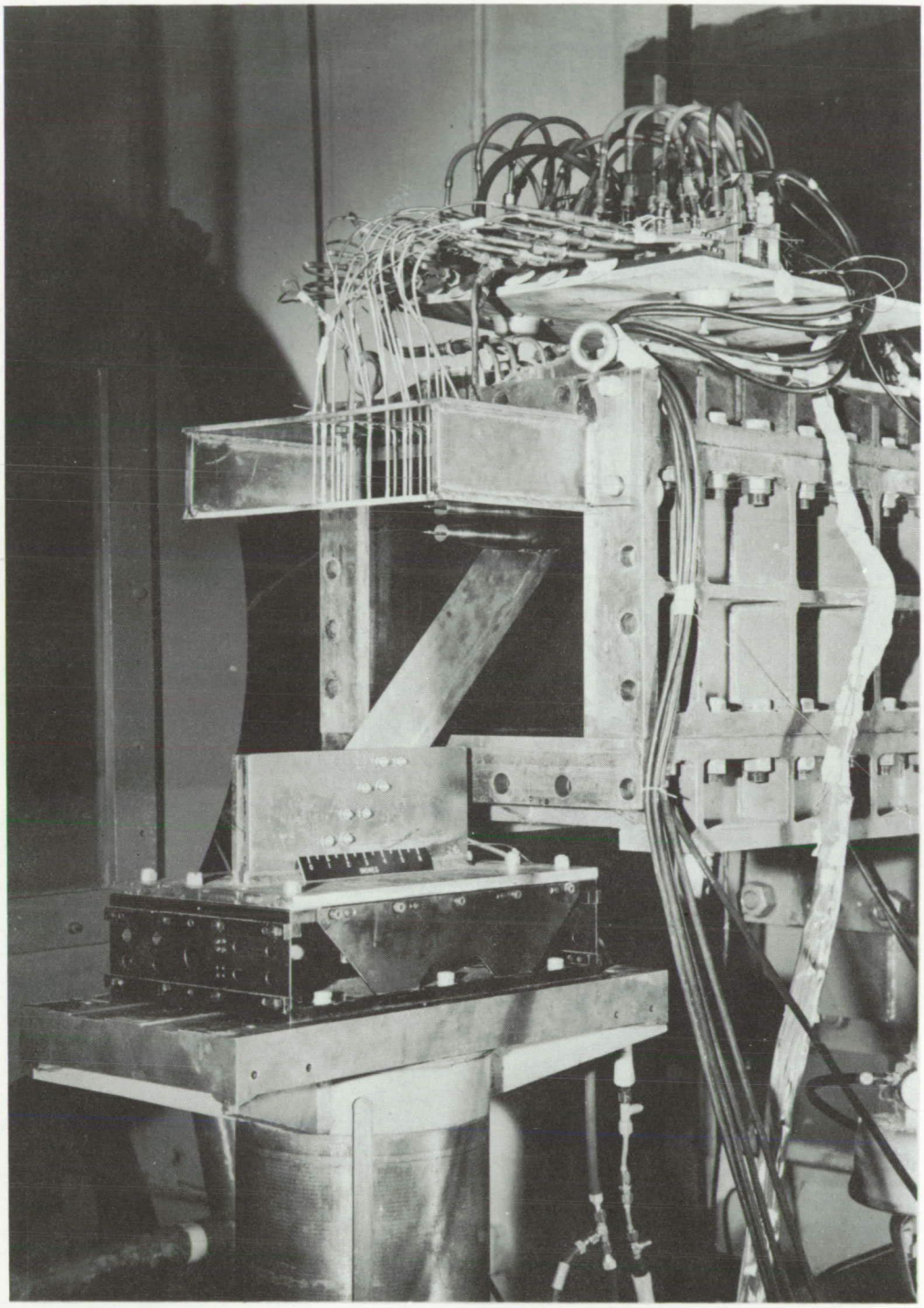

L-79061.1

Figure 1.- Photograph of the nacelle mounted beneath the flat-surface wing in the 12- by 12-inch preflight-jet nozzle.

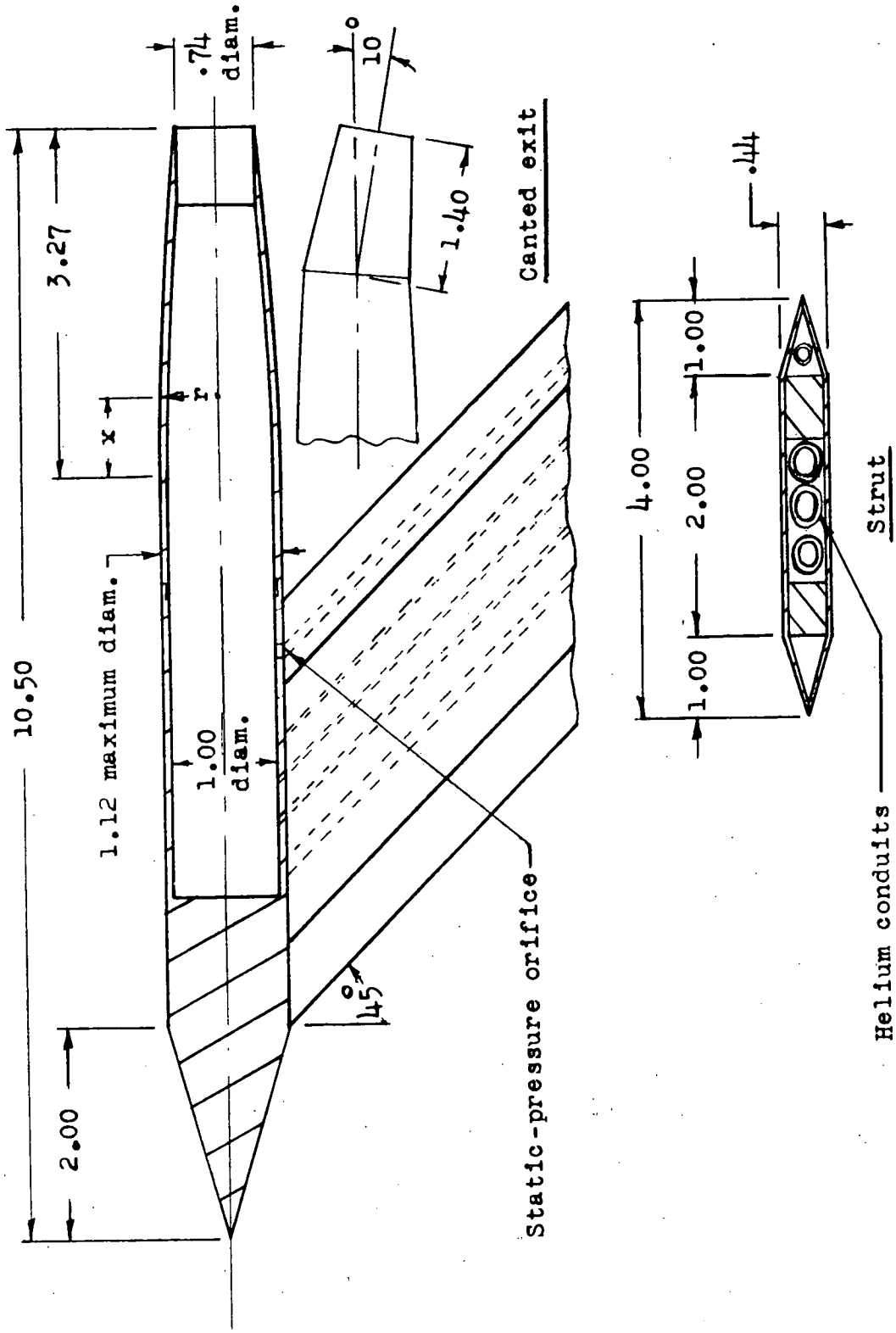

Figure 2.- Schematic diagram of nacelle. All dimensions are in inches.

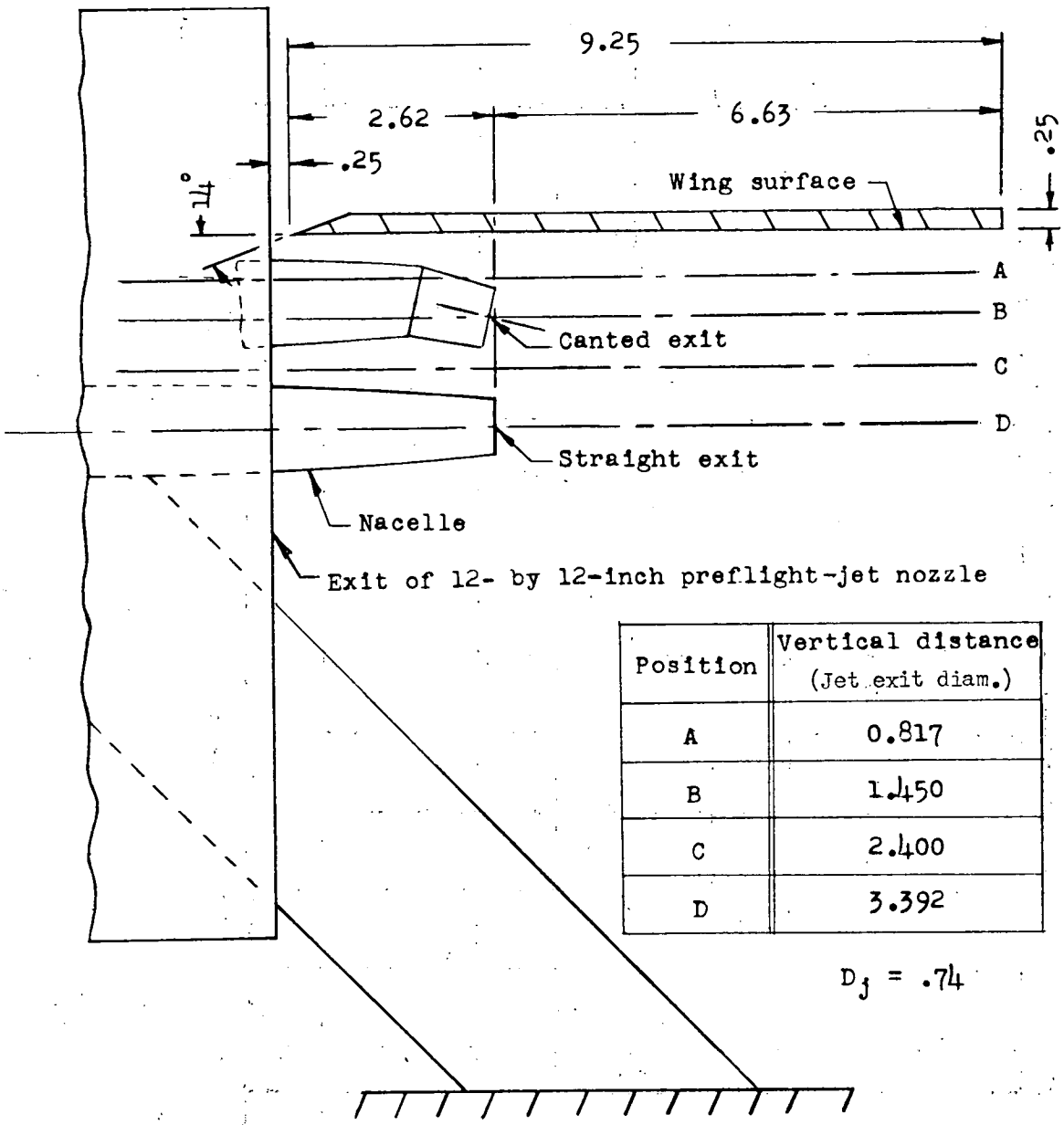

Position	Vertical distance (Jet exit diam.)
A	0.817
B	1.450
C	2.400
D	3.392

$D_j = .74$

Figure 3.- Arrangement of the nacelle relative to the exit of the 12- by 12-inch preflight-jet nozzle and wing for test positions A, B, C, and D. All dimensions are in inches.

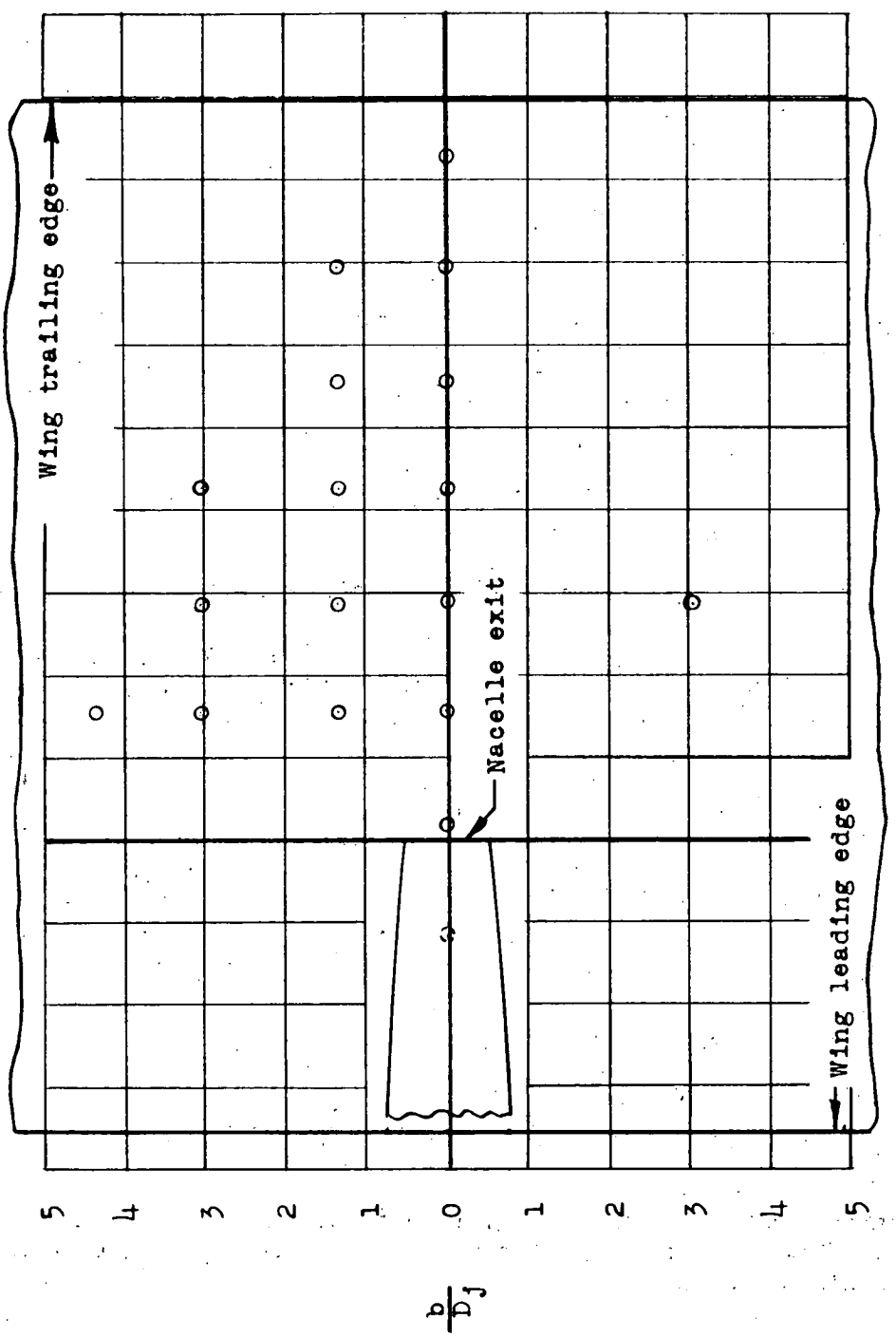

Figure 4.- Location of the wing static-pressure orifices.

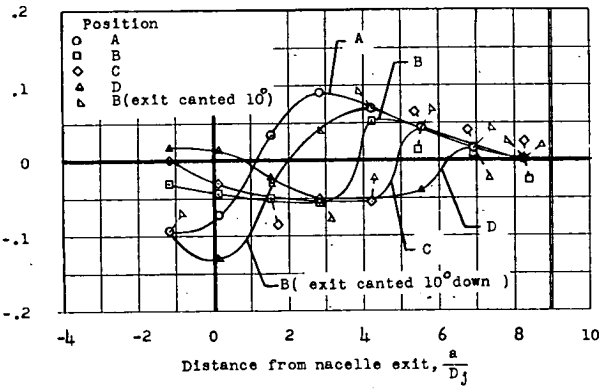

(a) Along nacelle center line.

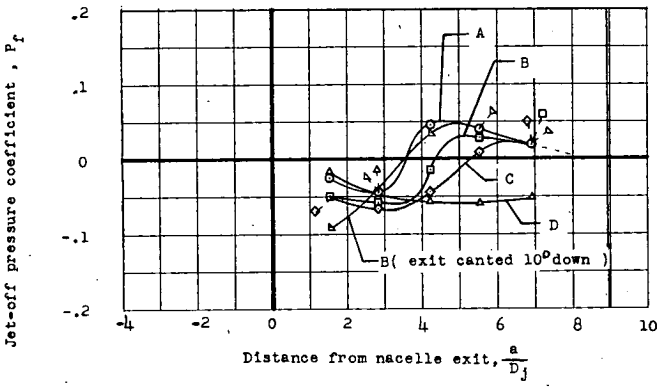

(b) $1.35D_j$ spanwise from nacelle center line.

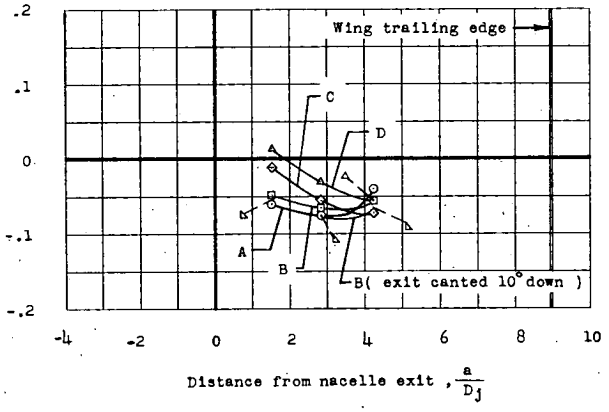

(c) $3.04D_j$ spanwise from nacelle center line.

Figure 5.- Chordwise variation of jet-off pressure coefficients for all test positions.

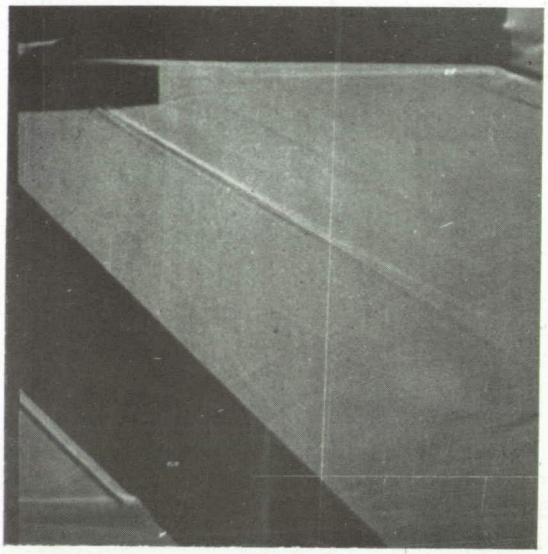

Position A

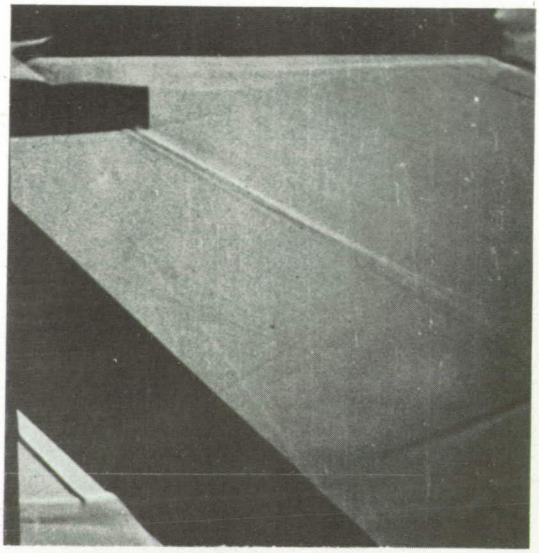

Position B

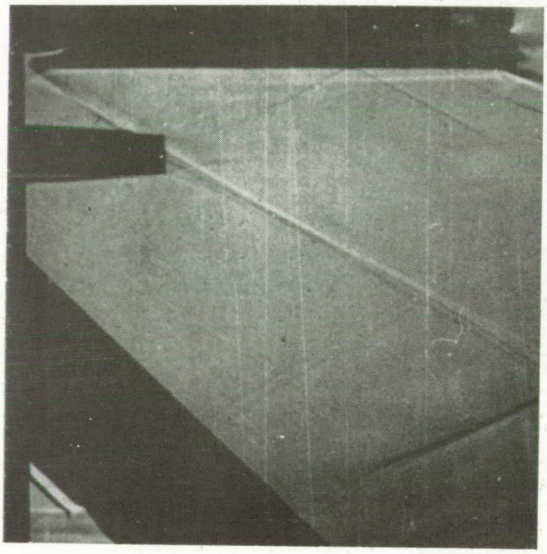

Position C

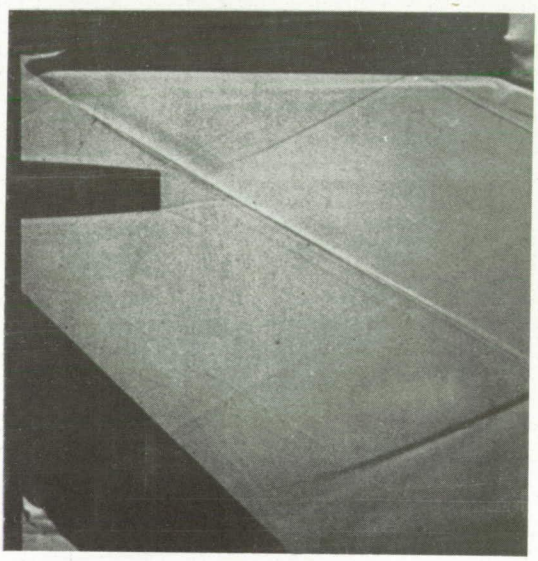

Position D

L-83670

Figure 6.- Shadowgraph pictures of the flow field about the nacelle exit with jet off for test positions A, B, C, and D.

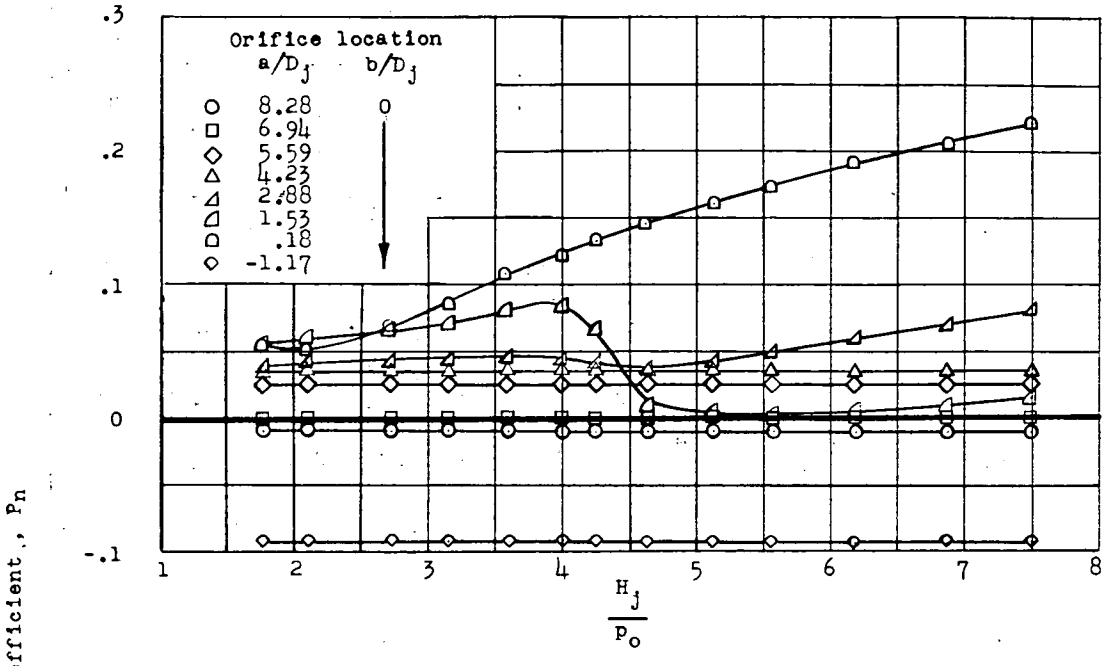

(a) Position A on nacelle center line.

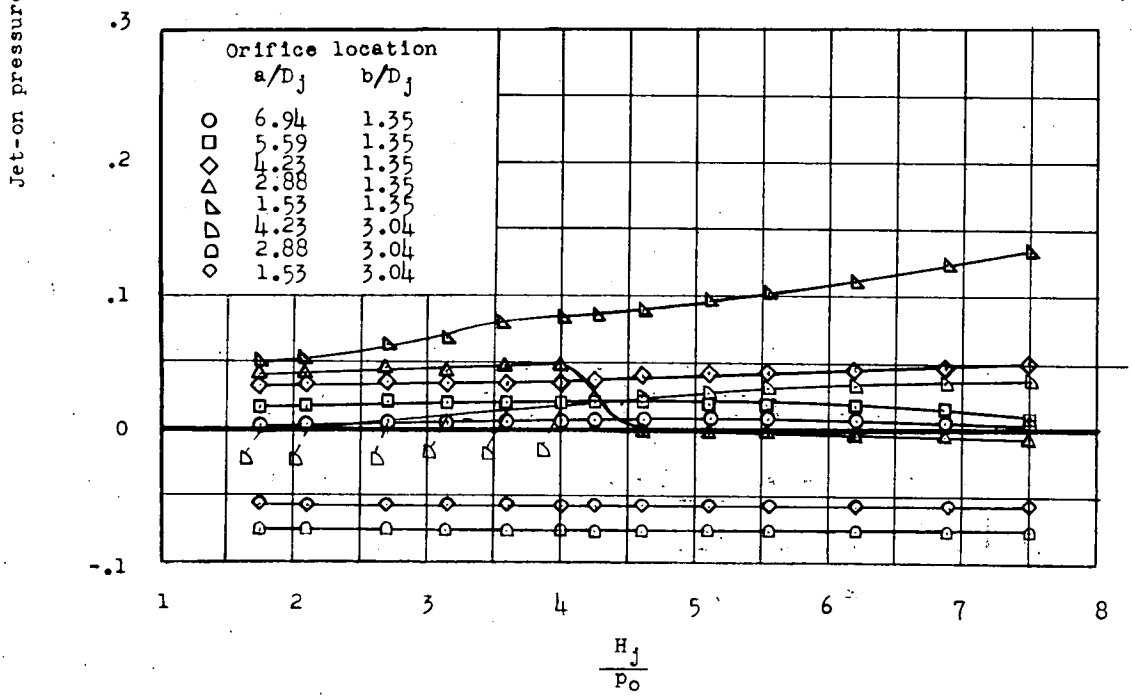

(b) Position A at $1.35D_j$ and $3.04D_j$ spanwise from nacelle center line.

Figure 7.- Variation of jet-on pressure coefficient with nacelle-exit pressure ratio for all wing pressure orifices.

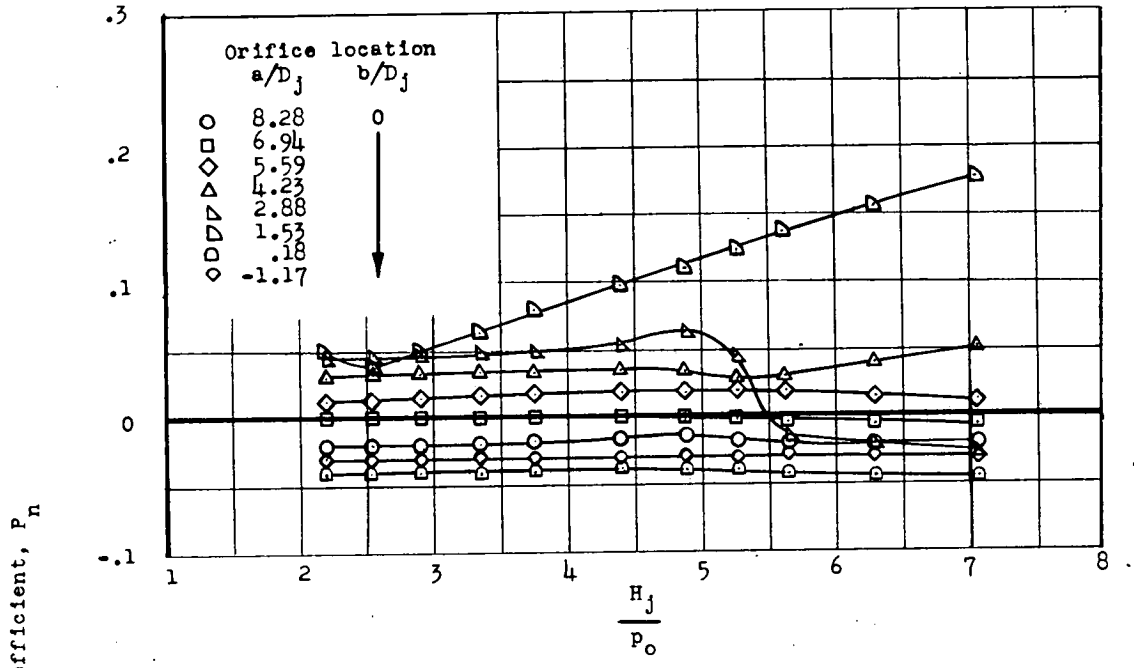

(c) Position B on nacelle center line.

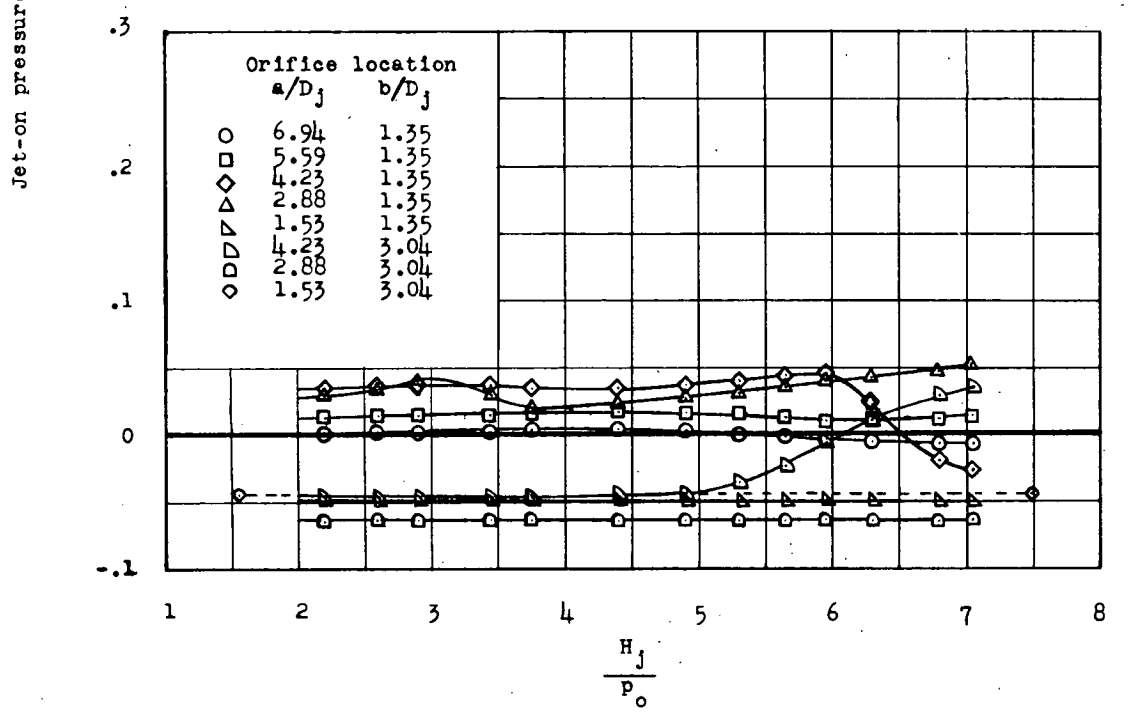

(d) Position B at $1.35D_j$ and $3.04D_j$ spanwise from nacelle center line.

Figure 7.- Continued.

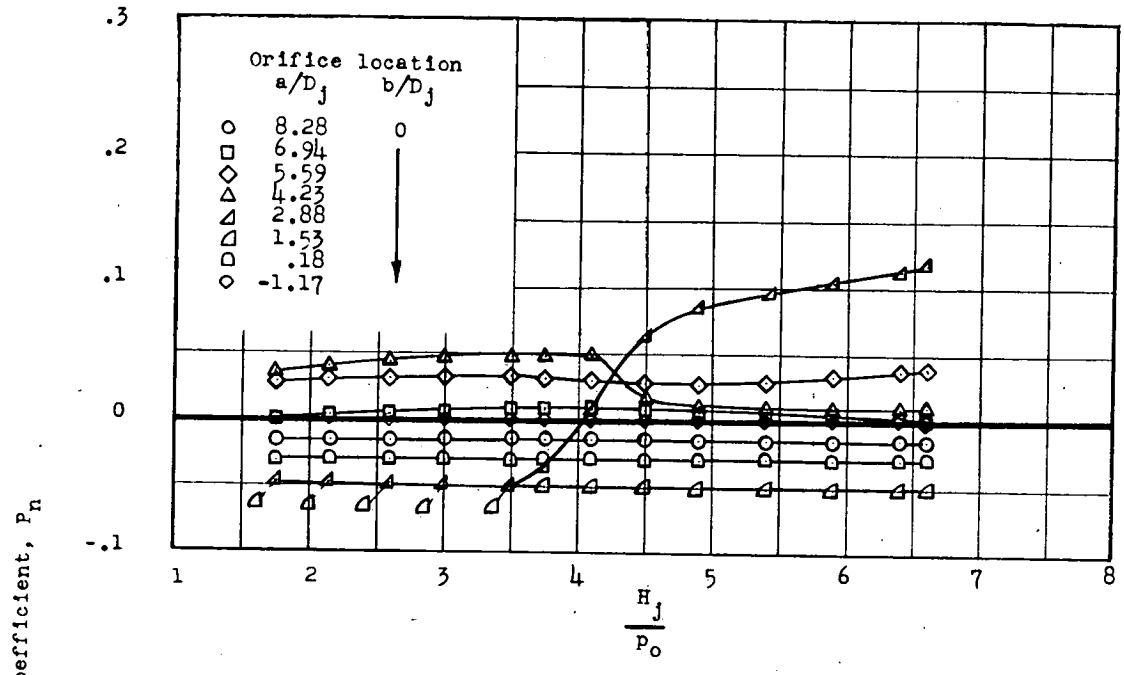

(e) Position C on nacelle center line.

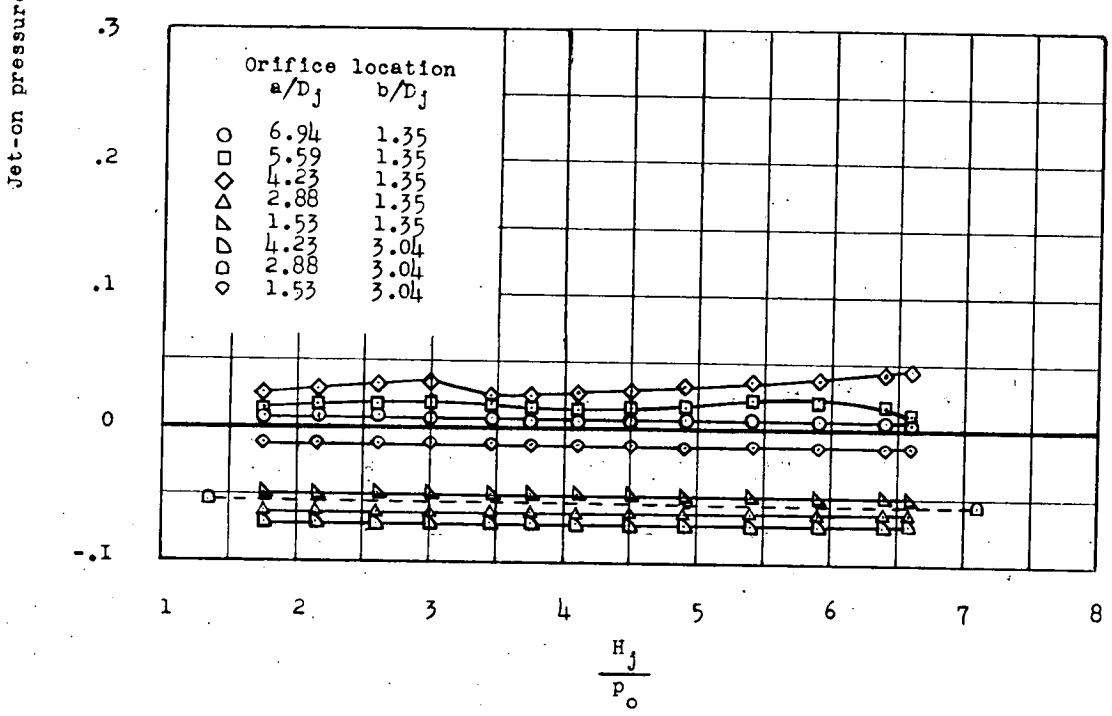

(f) Position C at $1.35D_j$ and $3.04D_j$ spanwise from nacelle center line.

Figure 7.- Continued.

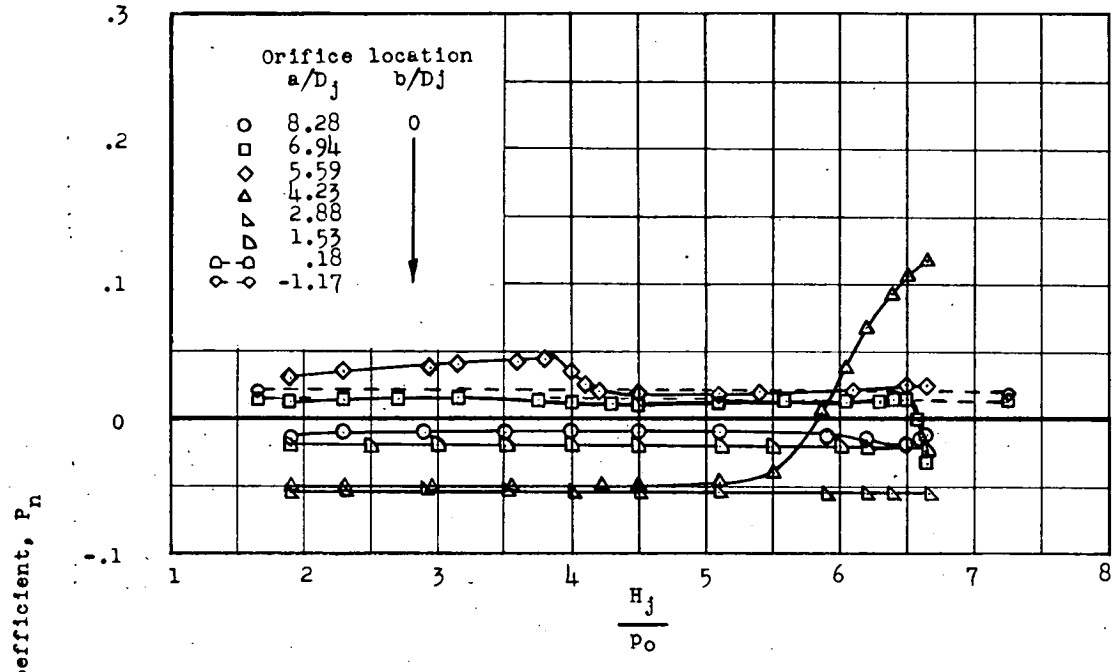

(g) Position D on nacelle center line.

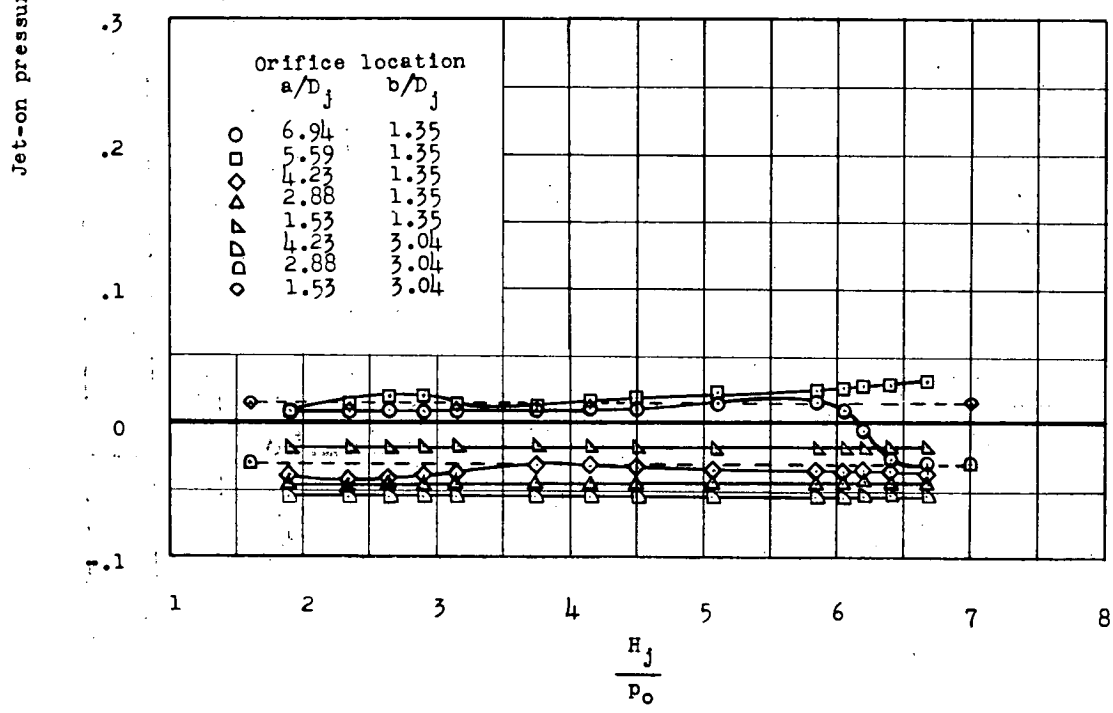

(h) Position D at $1.35D_j$ and $3.04D_j$ spanwise from nacelle center line.

Figure 7.- Continued.

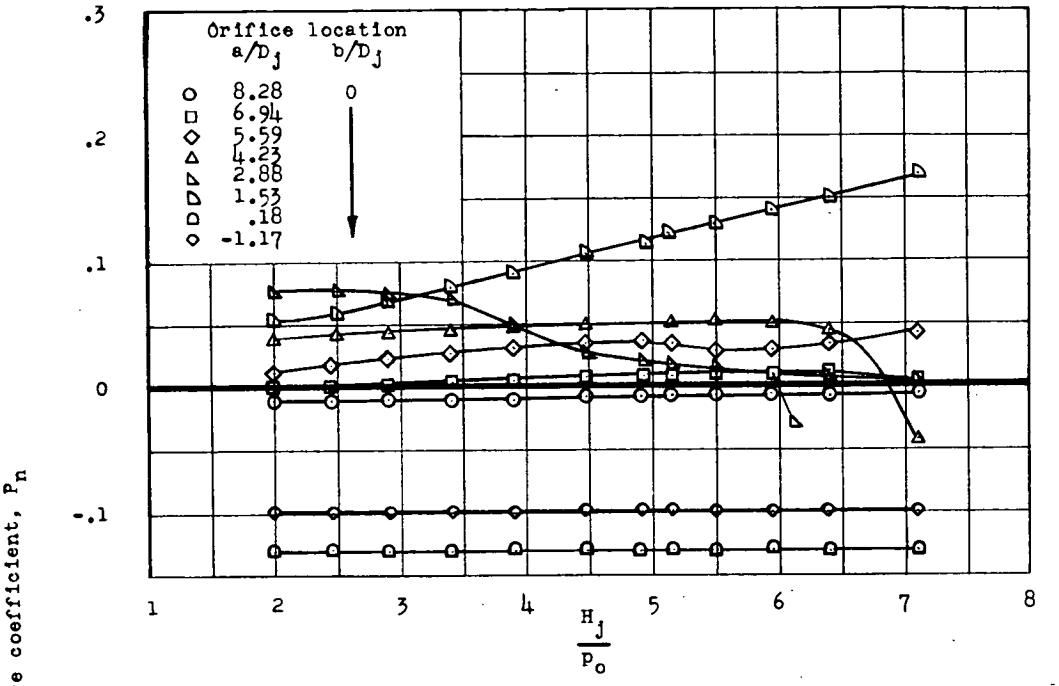

(i) Position B (exit canted 10° down) on nacelle center line.

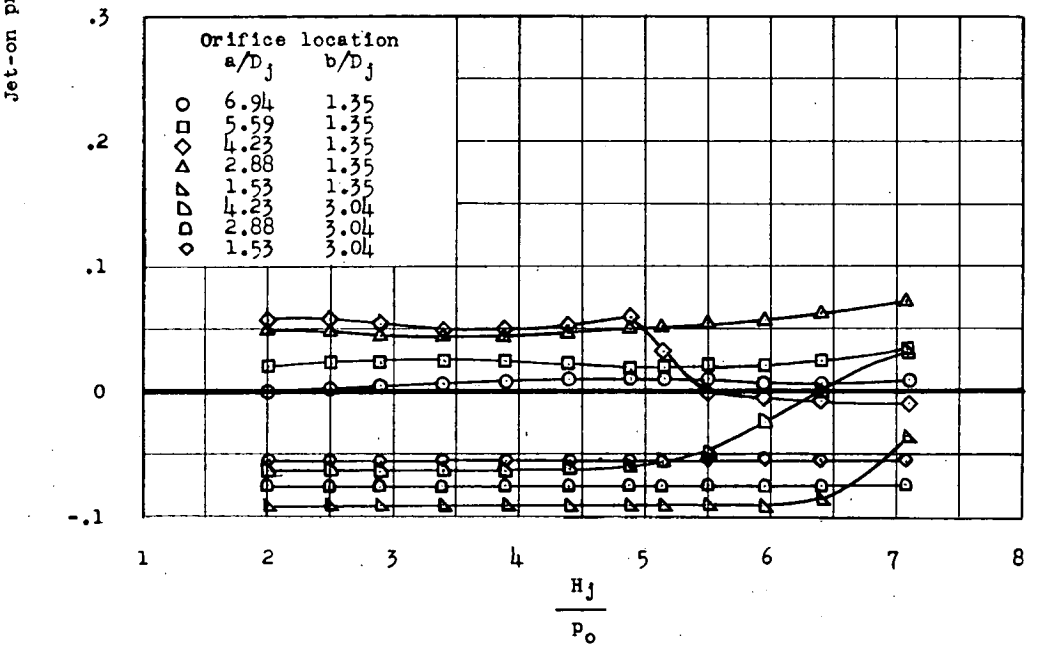

(j) Position B (exit canted 10° down) at $1.35D_j$ and $3.04D_j$ spanwise from nacelle center line.

Figure 7.- Concluded.

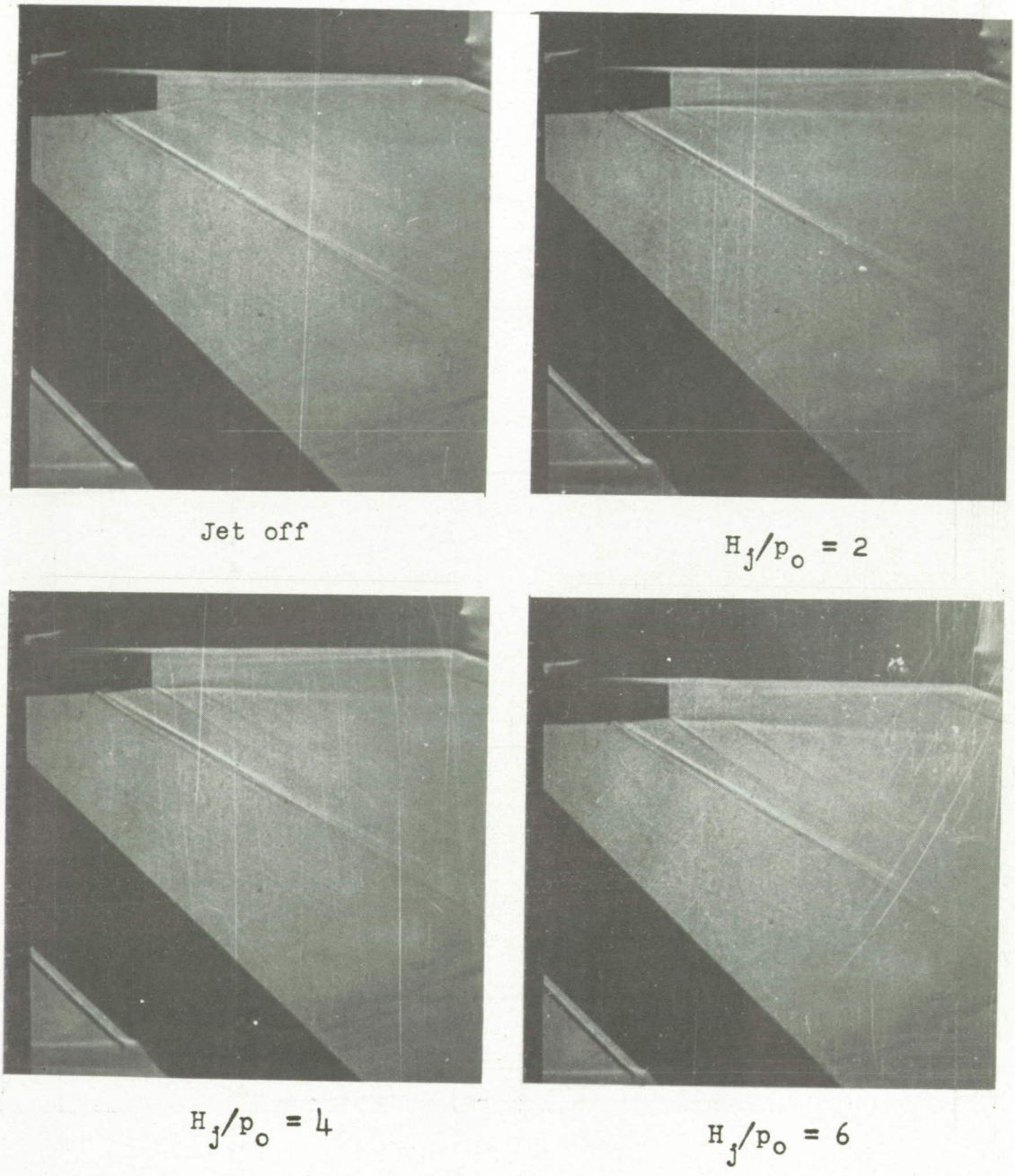

(a) Position A.

Figure 8.- Shadowgraph pictures of the flow field about the nacelle exit with jet off and with nacelle-exit pressure ratios of 2, 4, and 6 for test positions A, B, C, and D.

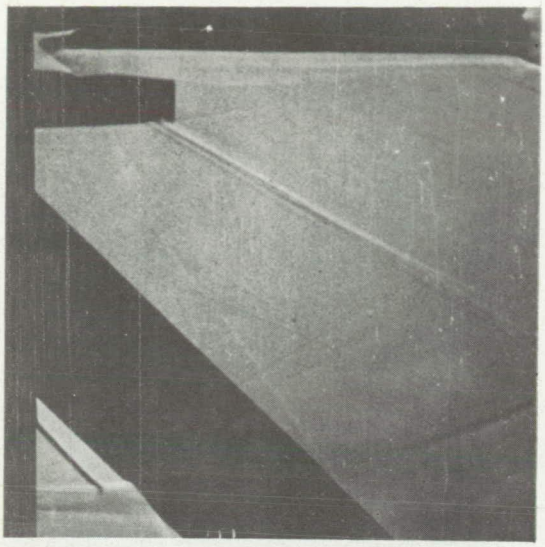

Jet off

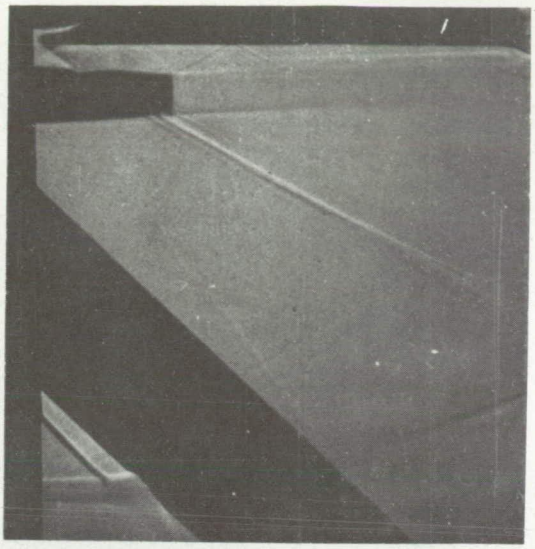

$H_j/p_o = 2$

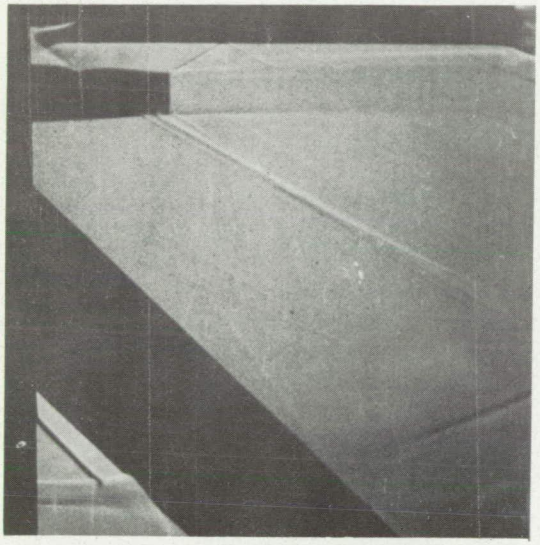

$H_j/p_o = 4$

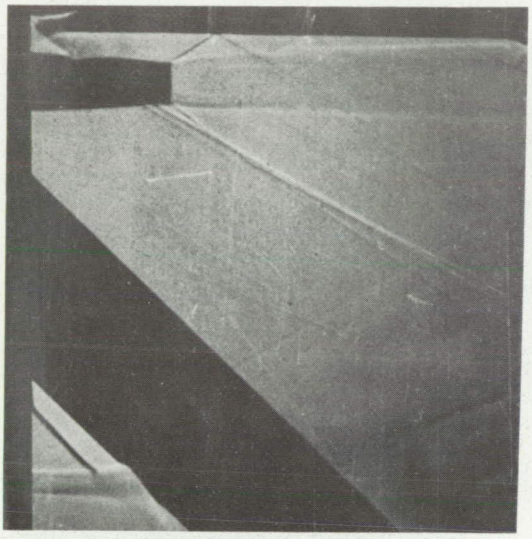

$H_j/p_o = 6$

L-83672

(b) Position B.

Figure 8.- Continued.

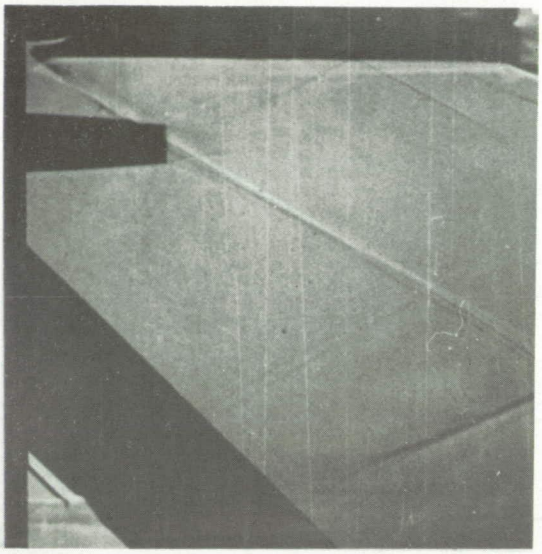

Jet off

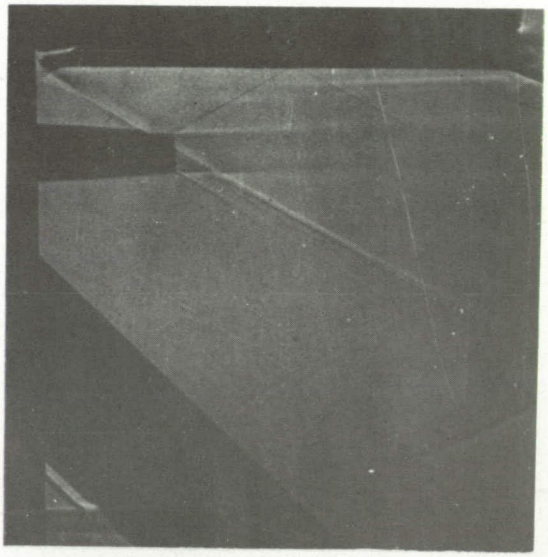

$H_j/p_o = 2$

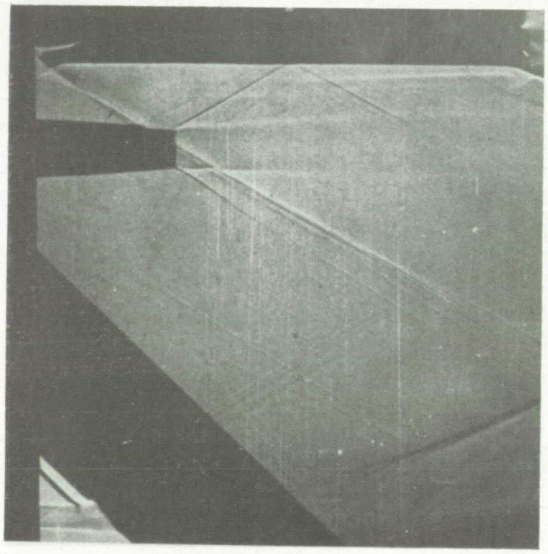

$H_j/p_o = 4$

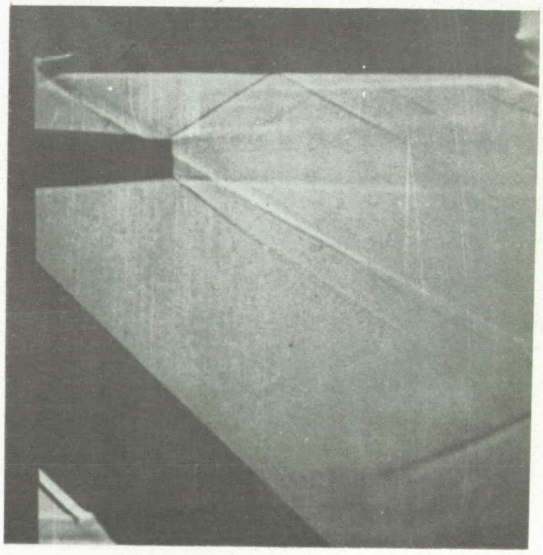

$H_j/p_o = 6$

L-83673

(c) Position C.

Figure 8.- Continued.

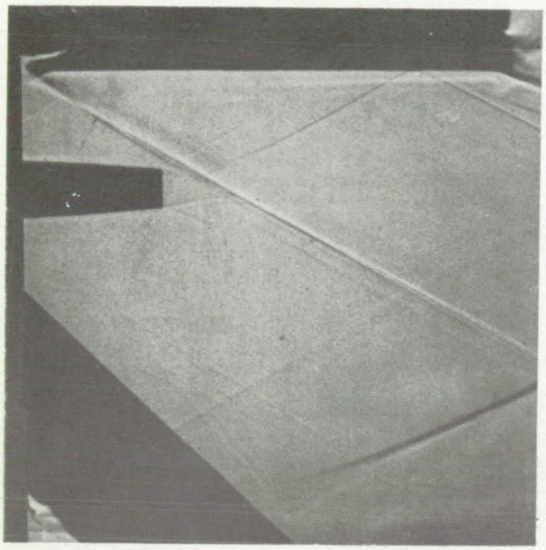

Jet off

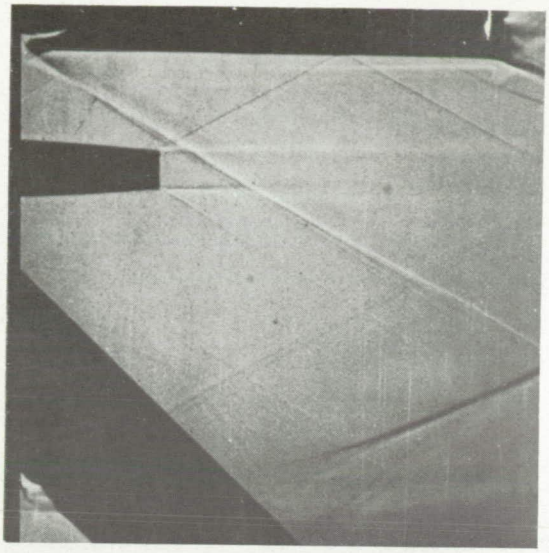

$H_j/p_o = 2$

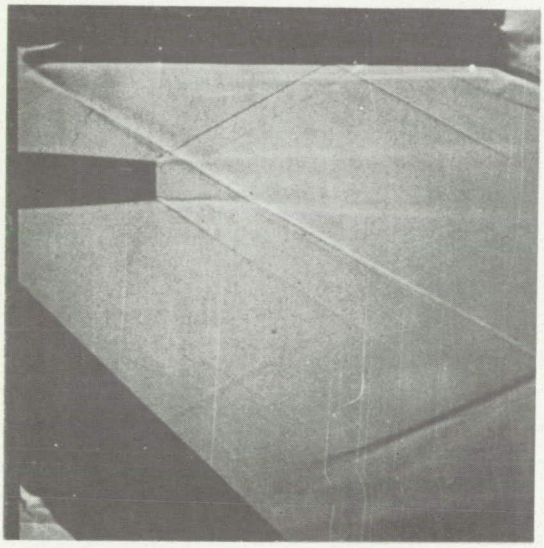

$H_j/p_o = 4$

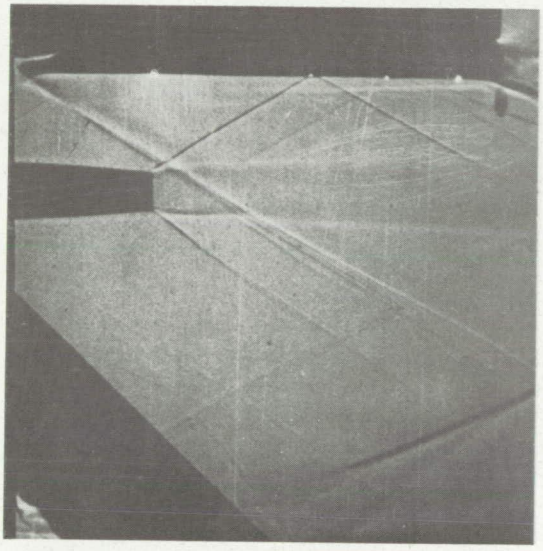

$H_j/p_o = 6$

L-83674

(d) Position D.

Figure 8.- Concluded.

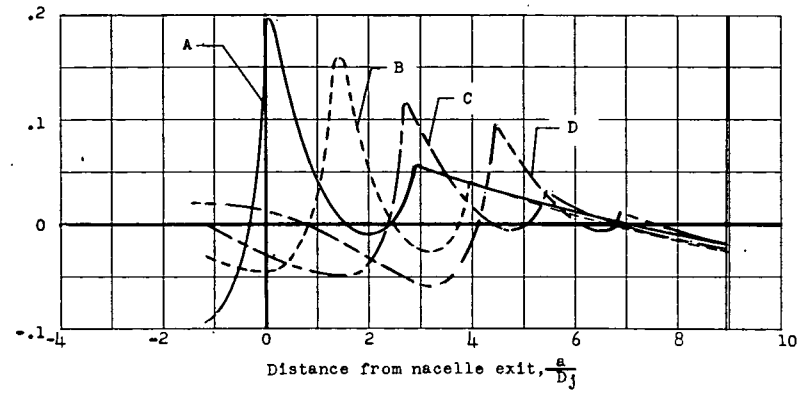

(a) Along nacelle center line.

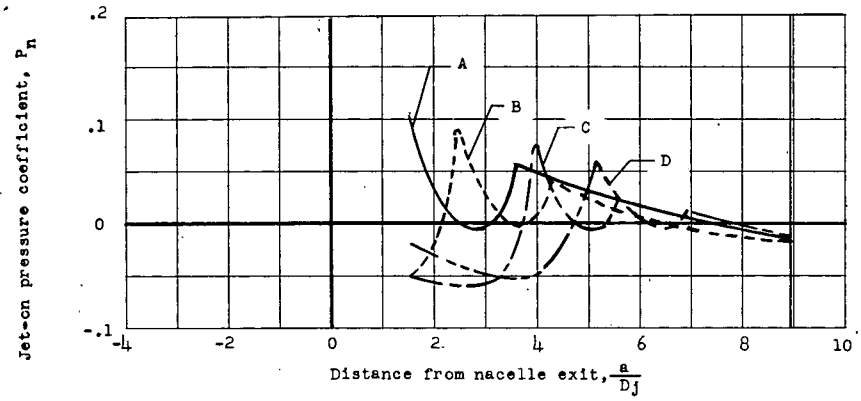

(b) $1.35D_j$ spanwise from nacelle center line.

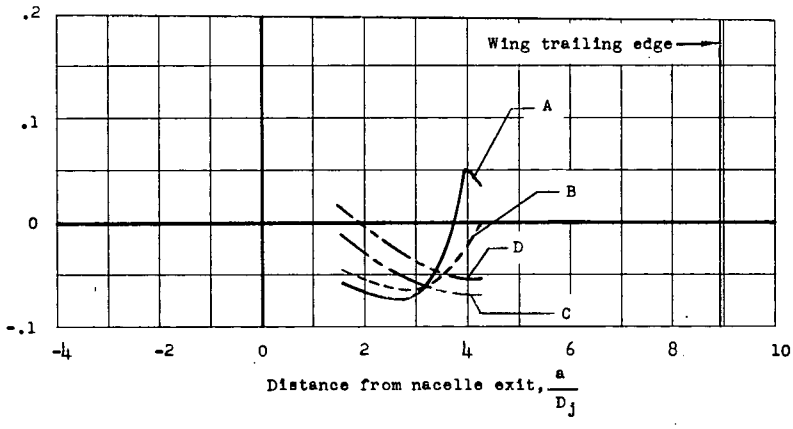

(c) $3.04D_j$ spanwise from nacelle center line.

Figure 9.- Chordwise variation of jet-on pressure coefficient for test positions A, B, C, and D at a nacelle-exit pressure ratio of 6.

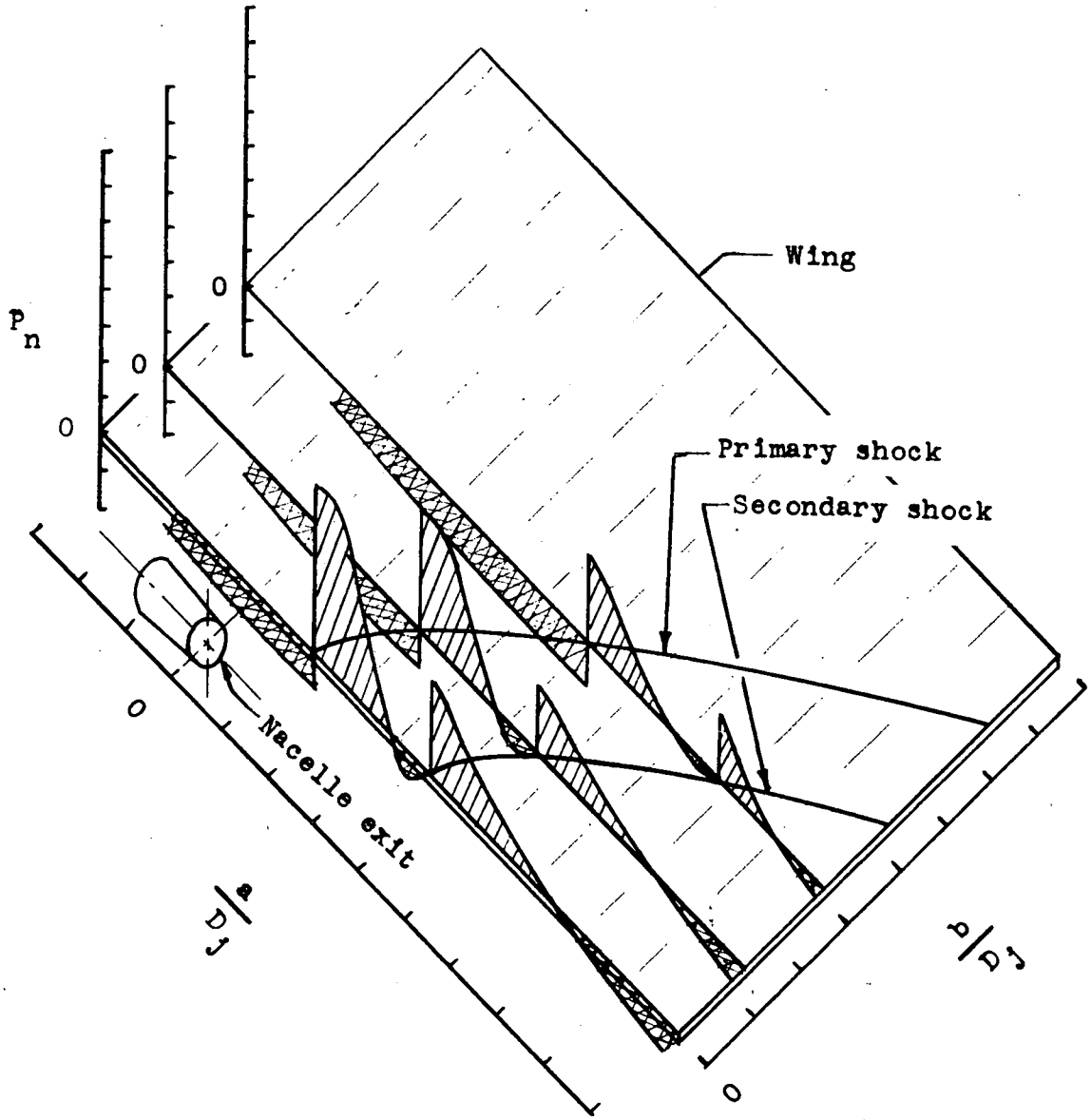

Figure 10.- Typical jet-on pressure field on the wing.

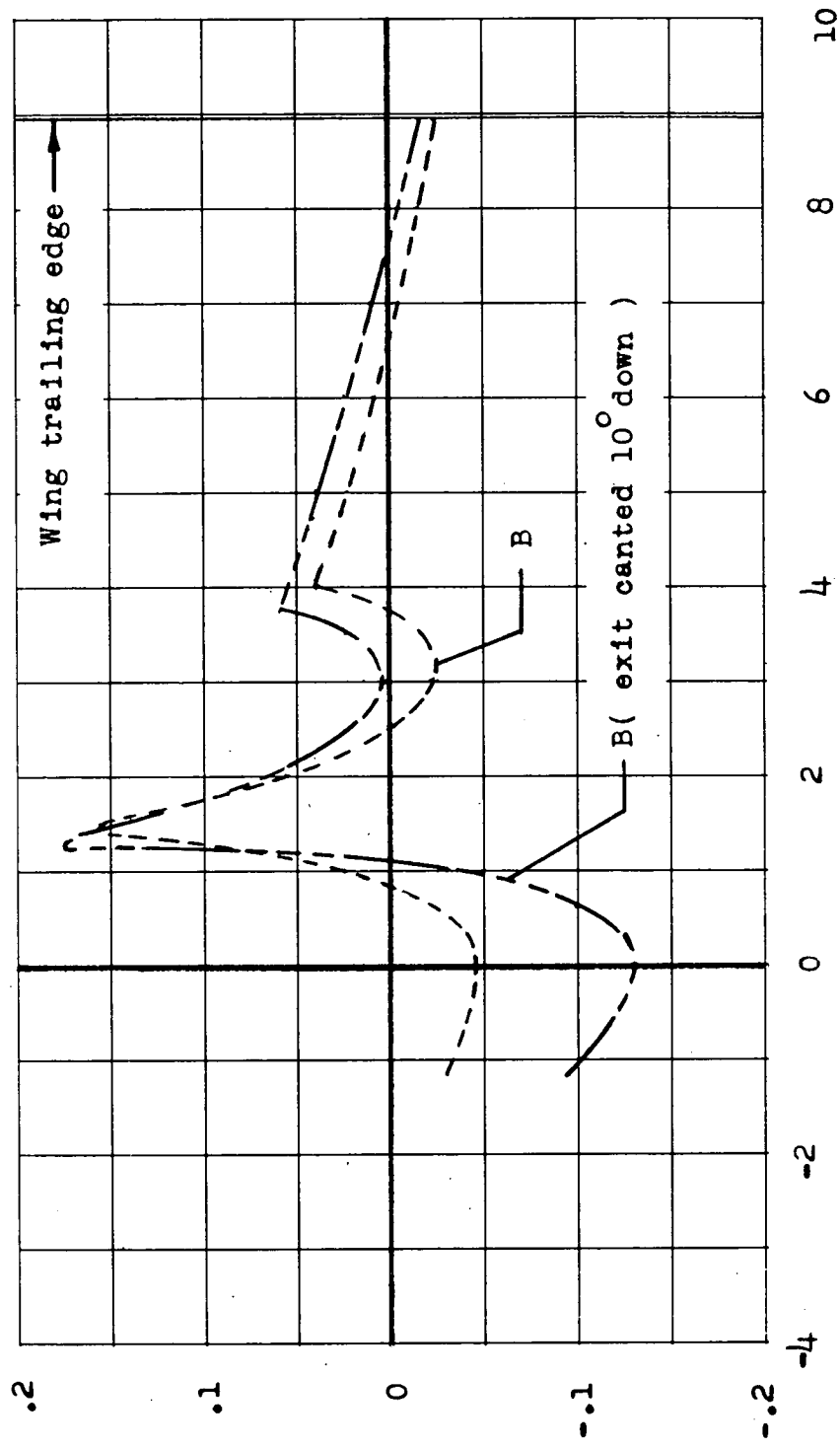

Figure 11.- Chordwise variation of jet-on pressure coefficient for test positions B and B (exit canted 10° down) at a nacelle-exit pressure ratio of 6 along the nacelle center line.

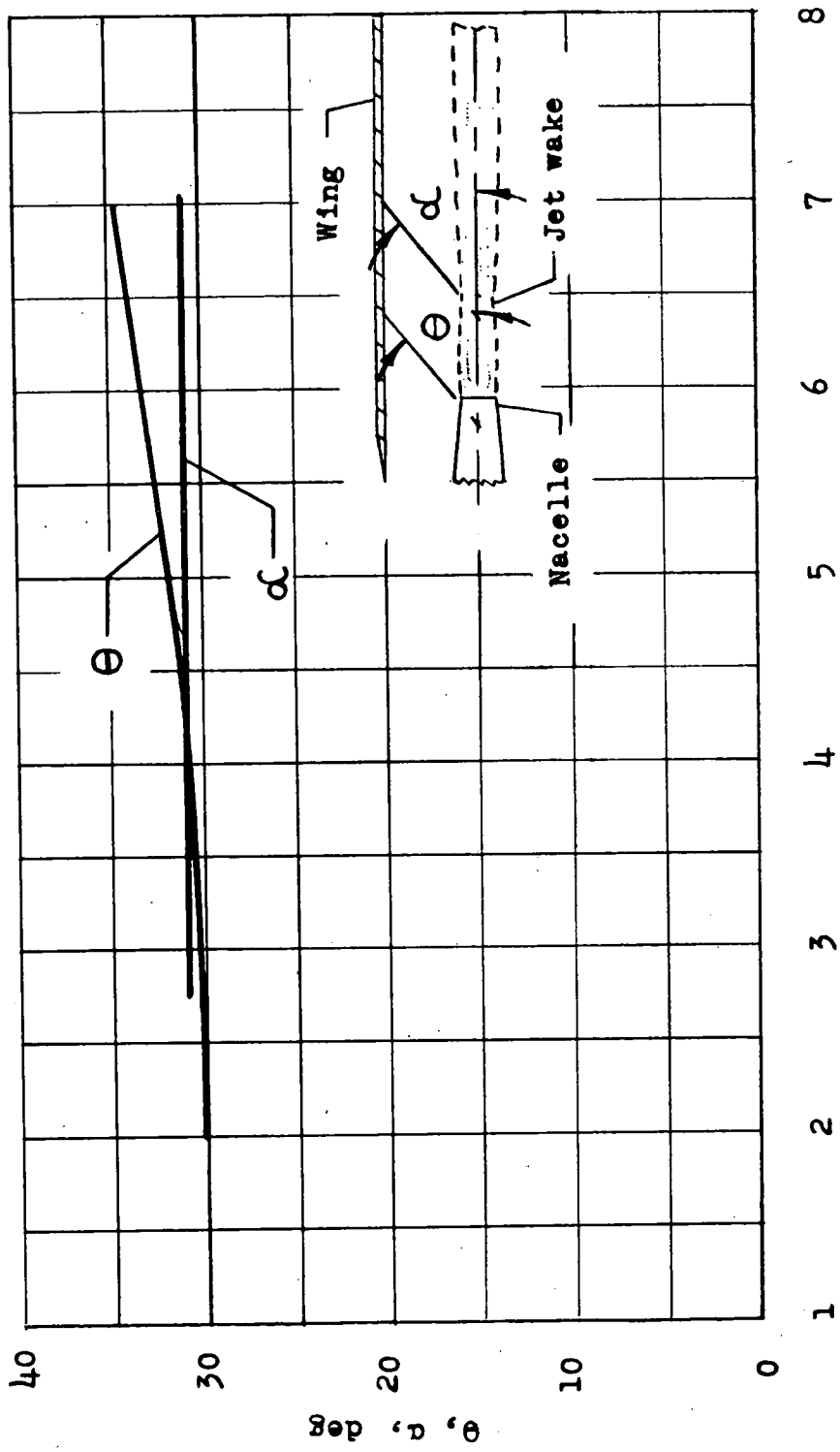

Figure 12.- Variation of primary and secondary jet-on shock-wave angles with nacelle-exit pressure ratio.

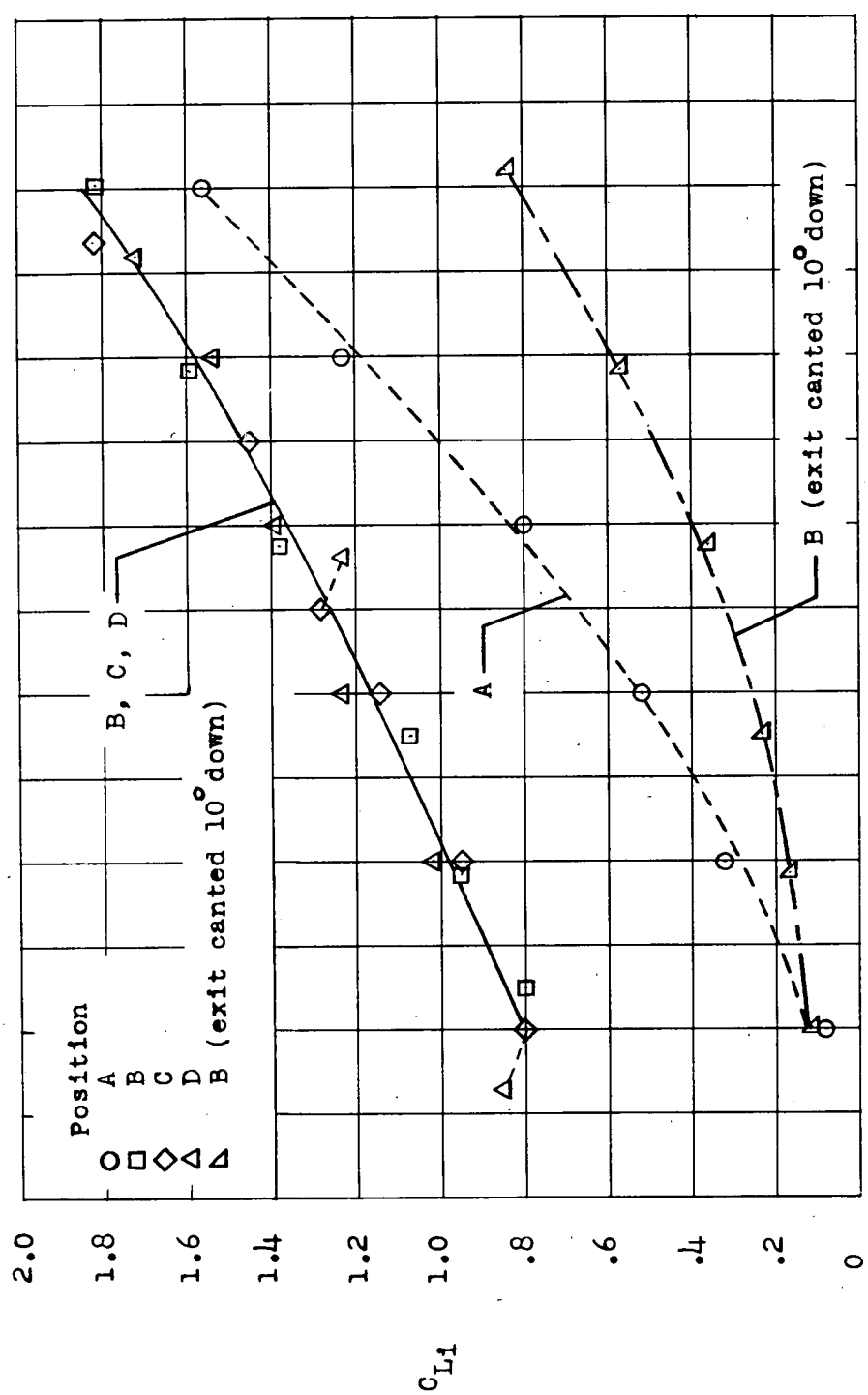

Figure 13.- Variation of incremental lift coefficient with nacelle-exit pressure ratio for all test positions, based on nacelle-exit area.

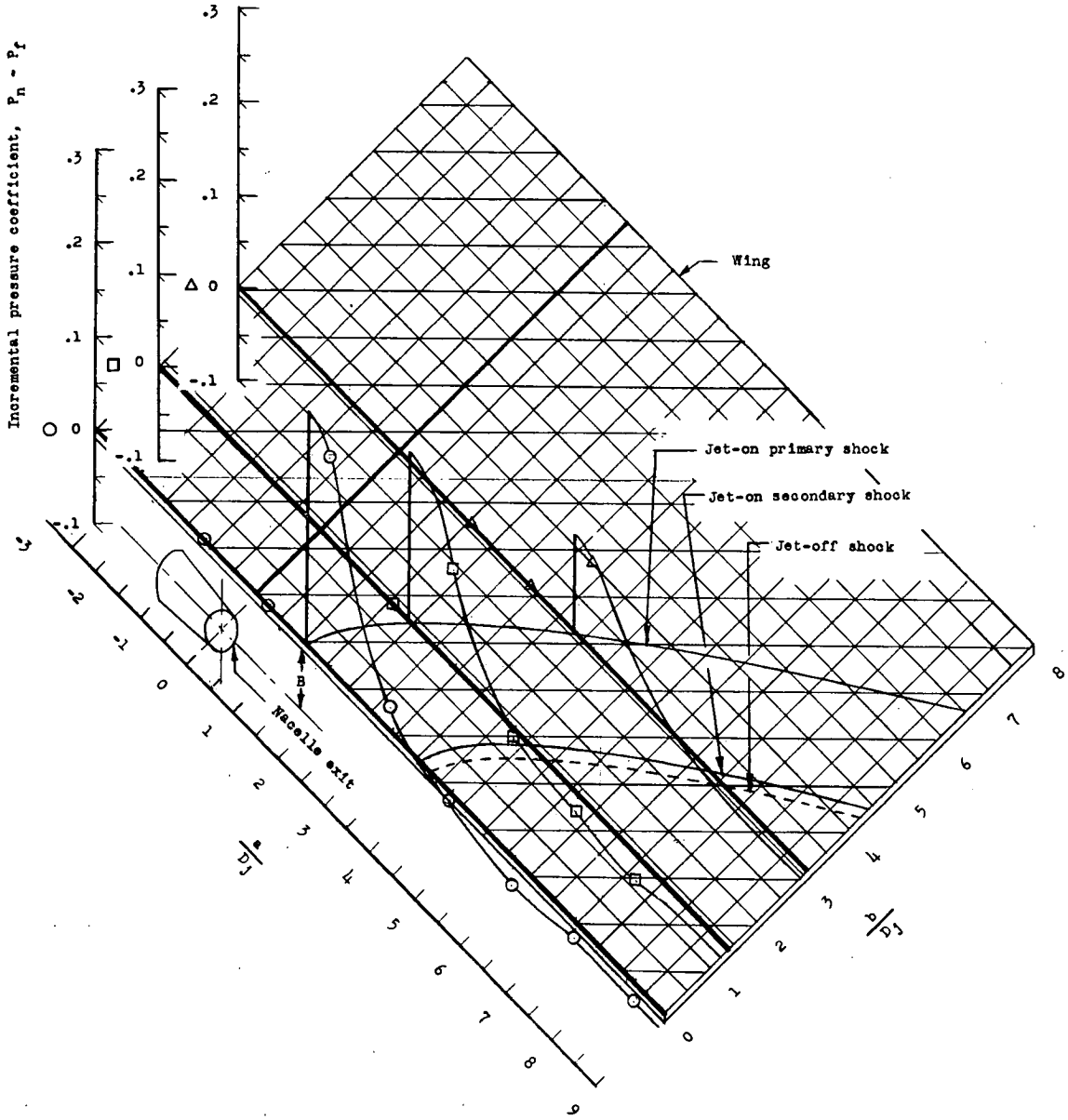

Figure 14.- Chordwise and spanwise variation of incremental pressure coefficient $P_n - P_f$ at test position B for a nacelle-exit pressure ratio of 7.

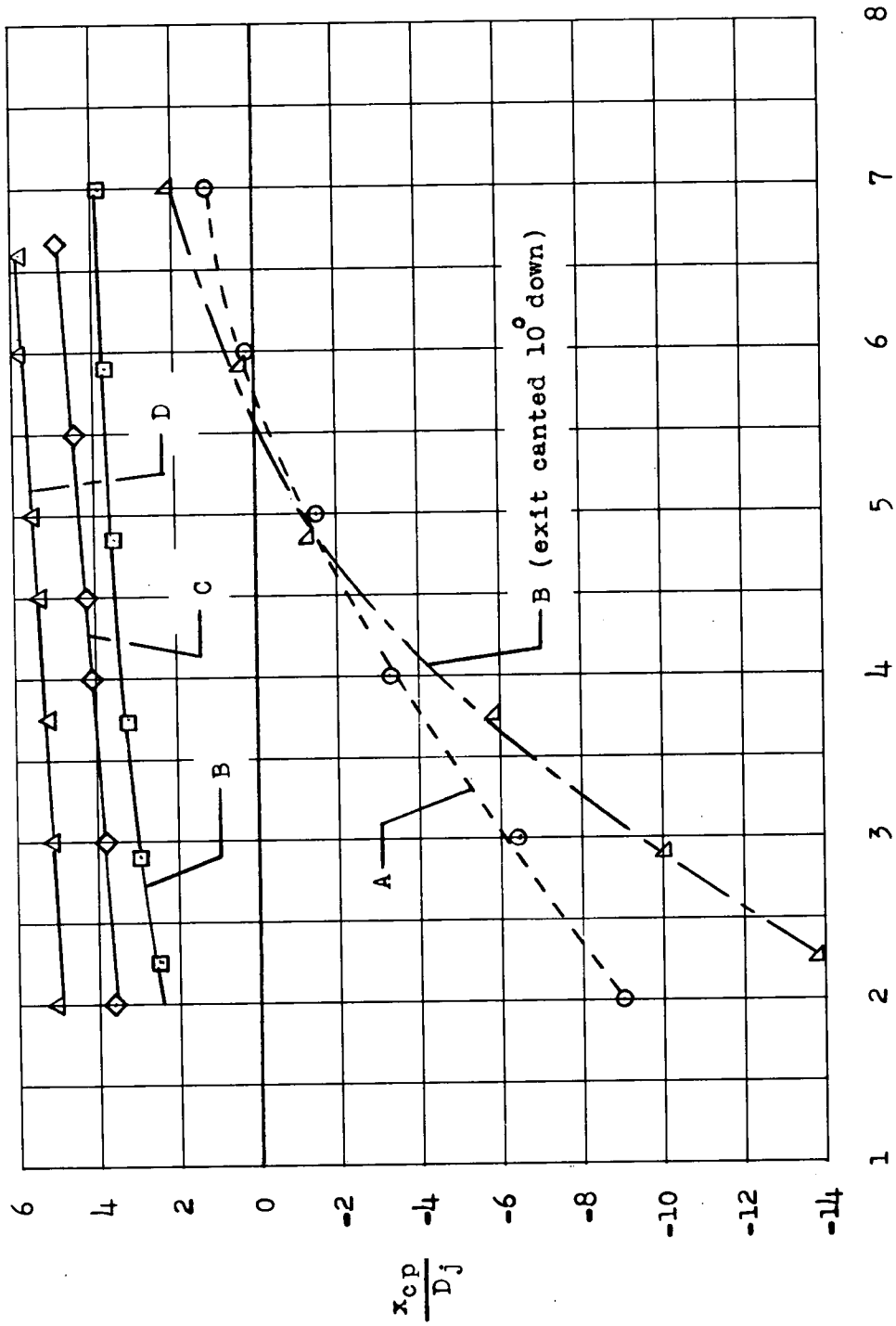

Figure 15.- Variation of the incremental-lift center of pressure with nacelle-exit pressure ratio for all test positions.

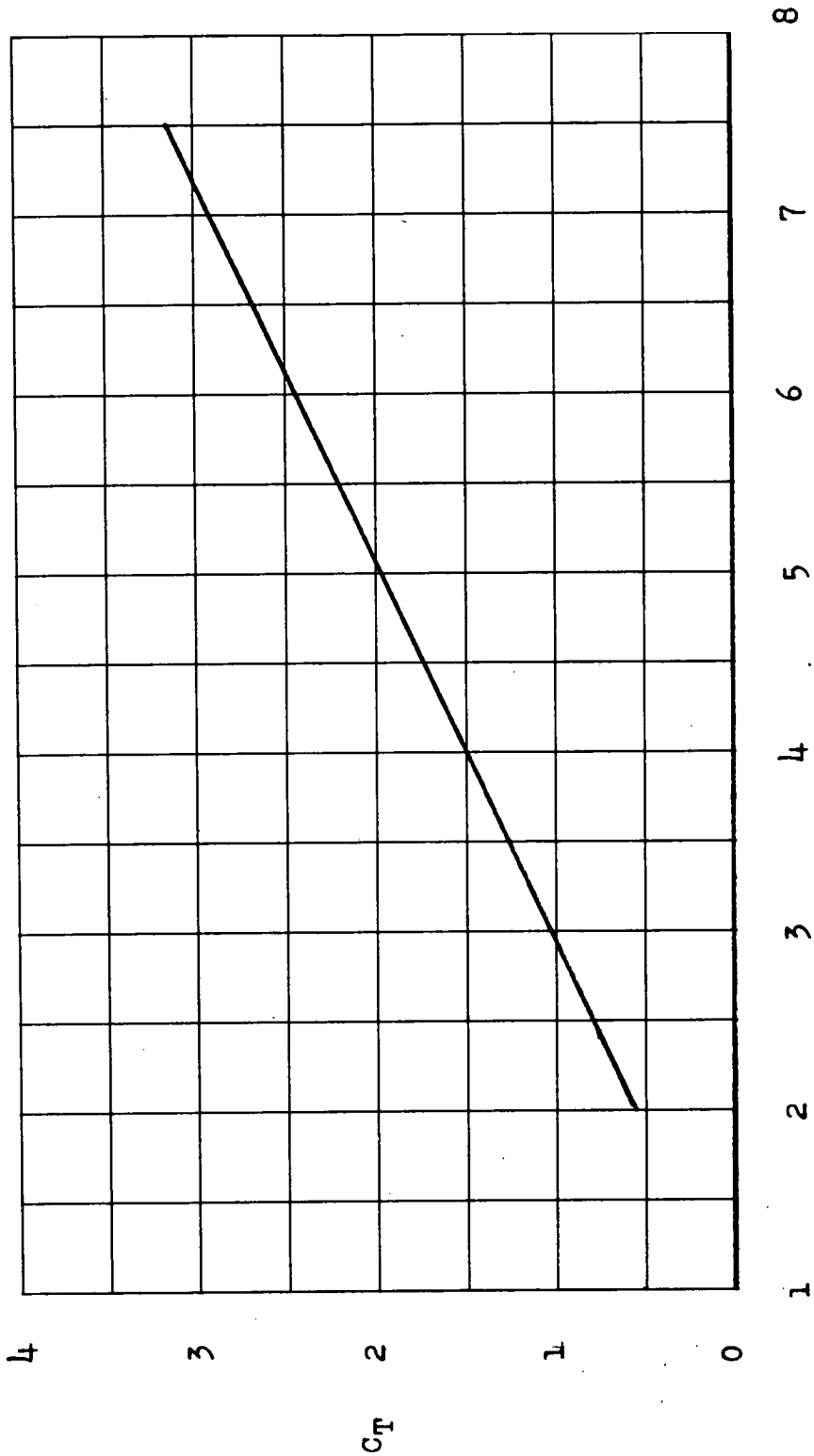

Figure 16.- Variation of gross thrust coefficient with nacelle-exit pressure ratio.

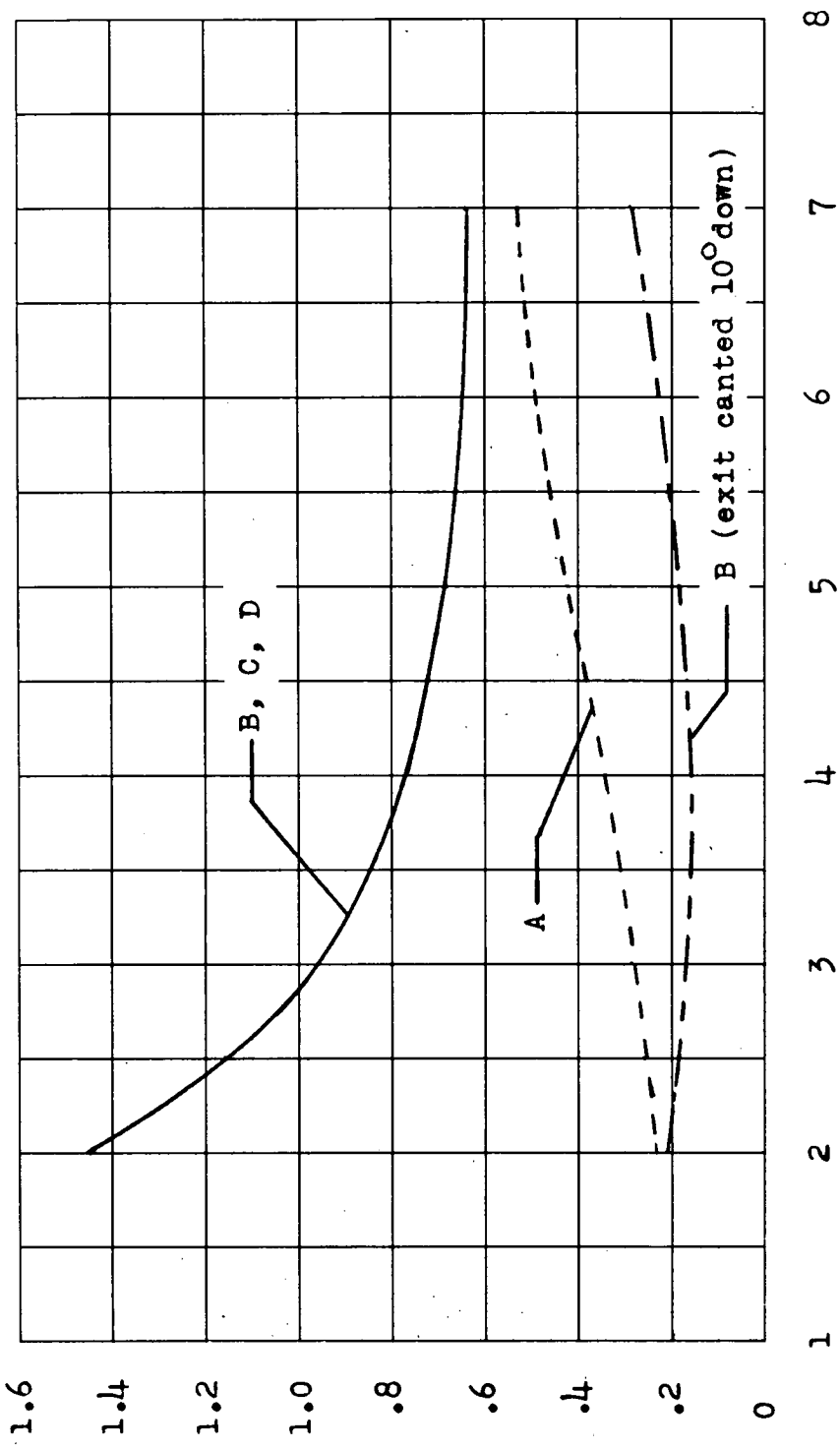

Figure 17.- Variation of the lift-to-thrust ratio with nacelle-exit pressure ratio.